Report Prepared by:

Mersedeh Akhoondan

Alberto A. Sagüés

FINAL REPORT

Corrosion of Spiral Rib Aluminized Pipe

Contract No. BDK84 977-11

Final Report to Florida Department of Transportation

A. A. Sagüés

Principal Investigator

Department of Civil and Environmental Engineering

University of South Florida

Tampa, FL 33620

August 2012

DISCLAIMER

The opinions, findings, and conclusions expressed in this publication are those of the authors and not necessarily those of the State of Florida Department of Transportation.

SI* (MODERN METRIC) CONVERSION FACTORS

APPROXIMATE CONVERSIONS TO SI UNITS

Symbol	When You Know	Multiply By	To Find	Symbol
		LENGTH		
in	inches	25.4	millimeters	mm
ft	feet	0.305	meters	m
yd	yards	0.914	meters	m
mi	miles	1.61	kilometers	km
		AREA		
in^2	square inches	645.2	square millimeters	mm^2
ft^2	square feet	0.093	square meters	m^2
yd^2	square yard	0.836	square meters	m^2
ac	acres	0.405	hectares	ha
mi^2	square miles	2.59	square kilometers	km^2
		VOLUME		
fl oz	fluid ounces	29.57	milliliters	mL
gal	gallons	3.785	liters	L
ft^3	cubic feet	0.028	cubic meters	m^3
yd^3	cubic yards	0.765	cubic meters	m^3
		NOTE: volumes greater than 1000 L shall be shown in m^3		
		MASS		
oz	ounces	28.35	grams	g
lb	pounds	0.454	kilograms	kg
T	short tons (2000 lb)	0.907	megagrams (or "metric ton")	Mg (or "t")
		TEMPERATURE (exact degrees)		
°F	Fahrenheit	5 (F-32)/9 or (F-32)/1.8	Celsius	°C
		ILLUMINATION		
fc	foot-candles	10.76	lux	lx
fl	foot-Lamberts	3.426	$candela/m^2$	cd/m^2
		FORCE and PRESSURE or STRESS		
lbf	poundforce	4.45	newtons	N
lbf/in^2	poundforce per square inch	6.89	kilopascals	kPa

APPROXIMATE CONVERSIONS FROM SI UNITS

Symbol	When You Know	Multiply By	To Find	Symbol
		LENGTH		
mm	millimeters	0.039	inches	in
m	meters	3.28	feet	ft
m	meters	1.09	yards	yd
km	kilometers	0.621	miles	mi
		AREA		
mm^2	square millimeters	0.0016	square inches	in^2
m^2	square meters	10.764	square feet	ft^2
m^2	square meters	1.195	square yards	yd^2
ha	hectares	2.47	acres	ac
km^2	square kilometers	0.386	square miles	mi^2
		VOLUME		
mL	milliliters	0.034	fluid ounces	fl oz
L	liters	0.264	gallons	gal
m^3	cubic meters	35.314	cubic feet	ft^3
m^3	cubic meters	1.307	cubic yards	yd^3
		MASS		
g	grams	0.035	ounces	oz
kg	kilograms	2.202	pounds	lb
Mg (or "t")	megagrams (or "metric ton")	1.103	short tons (2000 lb)	T
		TEMPERATURE (exact degrees)		
°C	Celsius	1.8C+32	Fahrenheit	°F
		ILLUMINATION		
lx	lux	0.0929	foot-candles	fc
cd/m^2	$candela/m^2$	0.2919	foot-Lamberts	fl
		FORCE and PRESSURE or STRESS		
N	newtons	0.225	poundforce	lbf
kPa	kilopascals	0.145	poundforce per square inch	lbf/in^2

*SI is the symbol for the International System of Units. Appropriate rounding should be made to comply with Section 4 of ASTM E380.

Technical Report Documentation Page

1. Report No.	2. Government Accession No.	3. Recipient's Catalog No.
4. Title and Subtitle CORROSION OF SPIRAL RIB ALUMINIZED PIPE		5. Report Date August 2012
		6. Performing Organization Code
7. Author(s) M. Akhoondan, A. A. Sagüés		8. Performing Organization Report No.
9. Performing Organization Name and Address Department of Civil and Environmental Engineering University of South Florida Tampa, FL 33620		10. Work Unit No. (TRAIS)
		11. Contract or Grant No. BDK84 977-11
12. Sponsoring Agency Name and Address Florida Department of Transportation 605 Suwannee St. MS 30 Tallahassee, Florida 32399 (850)414-4615		13. Type of Report and Period Covered FINAL REPORT (02/10/2010 - 08/01/2012)
		14. Sponsoring Agency Code
15. Supplementary Notes		

16. Abstract

Aluminized steel pipes are expected to have a long service life, e.g., 75 years. Spiral ribbed aluminized pipes (SRAP) have been widely specified and used by the Florida Department of Transportation (FDOT) for drainage of runoff water. Confidence in the long-term durability of SRAP has been challenged by recent unexpected early corrosion failures in various Florida locations. SRAP premature corrosion incidents have occurred in two modalities. Mode A has taken place in near-neutral soil environments and has been often associated with either gross manufacturing defects (i.e., helical cuts) or corrosion concentration at or near the ribs. Mode B took place in pipes in contact with limestone backfill, and corrosion damage was in the form of perforations, not preferentially at the ribs and not necessarily associated with other deficiencies. These failures motivated initial research as well as the continuation investigation reported here. The objectives of this work were to establish to what extent the Mode A corrosion incidents can be ascribed to manufacturing defects that can be rectified by appropriate quality control, as opposed to an intrinsic vulnerability to corrosion of regularly produced SRAP due to ordinary forming strains, and to determine the mechanism responsible for Mode B corrosion, including the role that limestone backfill played in that deterioration. To achieve those objectives, laboratory experiments were conducted to replicate the conditions for Mode A and Mode B. Overall, the findings of this and previous work suggest that much of the corrosion damage observed in the Mode A incidents was promoted more by manufacturing deficiencies and less by any possible inherent susceptibility of corrosion at the ribs of SRAP that is produced following appropriate quality control. Experiments to explore the causes of Mode B corrosion showed that high pH values, sufficient to cause dissolution of the passive film on aluminum, can develop under exposure of limestone to flowing natural water. The findings substantiate for the first time an important vulnerability of aluminized steel in limestone soils and provide an explanation for the onset of rapid deterioration observed in the field under Mode B. The findings also provide strong evidence in support of service guidelines to disallow the use of limestone bedding for aluminized steel pipe, including SRAP.

17. Key Words	18. Distribution Statement
Aluminized Steel Pipe, Corrosion, Spiral Rib, Corrugated, Culvert, Drainage, Limestone	This report is available to the public through the NTIS, Springfield, VA 22161

19. Security Classif. (of this report)	20. Security Classif. (of this page)	21. No. of Pages	22. Price
Unclassified	Unclassified	80	

ACKNOWLEDGEMENTS

The assistance with field inspections by Mario Paredes and many other collaborators at the FDOT State Materials Office is greatly appreciated, as is that of numerous student participants in the University of South Florida College of Engineering Research Experience for Undergraduates program and staff from the University of South Florida Nanotechnology Research and Education Center.

EXECUTIVE SUMMARY

Aluminized steel pipes are expected to have a long service life, e.g., 75 years. Aluminized steel corrosion resistance is provided mainly by a thermodynamically stable, thin passive film of aluminum oxide. If this film is damaged or removed by abrasion, another layer of oxide is expected to form rapidly and prevent further corrosion. Spiral ribbed aluminized pipes (SRAP) have good hydraulic efficiency and structural strength. Therefore, SRAP have been widely specified and used by the Florida Department of Transportation (FDOT) for drainage of runoff water.

Confidence in the long-term durability of SRAP has been challenged by recent unexpected early corrosion failures in various Florida locations. SRAP premature corrosion incidents have occurred in two modalities. Mode A has taken place in near-neutral soil environments and has been often associated with either gross manufacturing defects (i.e., helical cuts) or corrosion concentration at or near the ribs. Mode A was first reported in 2005 for the drainage system owned by the city of St. Cloud, FL. The affected pipes were installed only about two years earlier.

Mode B took place in pipes in contact with limestone backfill, and corrosion damage was in the form of perforations, not preferentially at the ribs and not necessarily associated with other deficiencies. Mode B failure has been documented so far in one location, SR 212 in Jacksonville, Florida, and was revealed in 2009 by video inspection of the installed pipes. The pipes had been in service for only three years. The corrosion was in the form of multiple localized pipe wall penetrations, starting from the soil side, over a section of pipe that was placed on a limestone backfill.

These failures motivated initial research (FDOT Project No. BD497) as well as the continuation investigation reported here. The objectives of this work were as follows:

- Establish to what extent the Mode A corrosion incidents can be ascribed to manufacturing defects that can be rectified by appropriate quality control, as opposed to an intrinsic vulnerability to corrosion of regularly produced SRAP due to ordinary forming strains

- Determine the mechanism responsible for Mode B corrosion and the role that limestone backfill played in that deterioration.

To achieve those objectives, laboratory experiments were conducted to replicate the conditions for Mode A and Mode B. Severe corrosion comparable to that of Mode A was observed in severely deformed aluminized steel. However, moderately strong deformation such as that involved in the normal forming of SRAP ribs did not consistently result in severe corrosion. In comparison tests, SRAP showed some rib corrosion but overall did not perform markedly differently from regular corrugated pipe, which is not subject to as much forming as SRAP. Experiments also confirmed that aluminized coating provides some galvanic protection to steel exposed at places of mechanical distress. However, the protection was limited and was not enhanced in lower resistivity environments.

Overall, the findings of this and previous work suggest that much of the corrosion damage observed in Mode A incidents was promoted more by manufacturing deficiencies and less by any possible inherent susceptibility of corrosion at the ribs of SRAP that is produced following appropriate quality controls.

Experiments to explore the causes of Mode B corrosion showed that high pH values, sufficient to cause dissolution of the passive film on aluminum, can develop under exposure of limestone to flowing natural water. In these conditions, extensive loss of coating was observed over a short time period. In contrast, exposure to water in contact with sand did not result in alkaline conditions, and aluminized steel, in the absence of mechanical deformation, remained essentially corrosion free.

The findings substantiate for the first time an important vulnerability of aluminized steel in limestone soils and provide an explanation for the onset of rapid deterioration observed in the field under Mode B. The findings also provide strong evidence in support of service guidelines to disallow the use of limestone bedding for aluminized steel pipe, including SRAP.

TABLE OF CONTENTS

LIST OF FIGURES

LIST OF TABLES

1. INTRODUCTION

1.1 Background

1.1.1 Aluminized Steel Pipe

Structural performance of metal drainage pipes is affected by abrasion, the backfill operations, improper choice of backfill material selection, presence of groundwater, level of compaction and compaction equipment used, and corrosion (Najafi et al., 2008). Premature replacement of buried metallic components is costly not only because of the price of the new unit, but also because of the associated road demolition and service outage. Of the factors mentioned above, corrosion is a key source of long-term deterioration. It is important to have in place reliable means of anticipating the extent of corrosion damage so that materials selection commensurate with the desired service life is made. This work is focused on better evaluating the corrosion performance of aluminized steel pipes, for which some unexpected corrosion damage incidents have occurred in recent years. This investigation is a continuation of an initial research project aimed at identifying the causes of that deterioration, under FDOT Project BD497. The findings of that work are detailed in its final report (Sagüés et al., 2009), to which reference is made throughout this document.

Aluminized steel type 2 (AST2) is produced as a steel sheet, hot-dip coated on both sides with commercially pure aluminum (ASTM A929 (ASTM 2007)) and AASHTO M274 (AASHTO 2008)). The process results in a dual coating, with an inner intermetallic brittle layer ~15 μm thick composed of Fe_2Al_5 (Kobayashi and Yakou, 2001) formed next to the low carbon steel substrate, and a nearly pure outer soft aluminum-matrix layer ~30 μm thick (Figure 1). The outer layer contains intermetallic precipitates with a 6-11 wt% Fe content (Cáseres and Sagüés, 2005). Those precipitates constitute ~5% of the volume of the outer layer. A full description of the aluminizing process appears in the previous report (Sagüés et al., 2009).

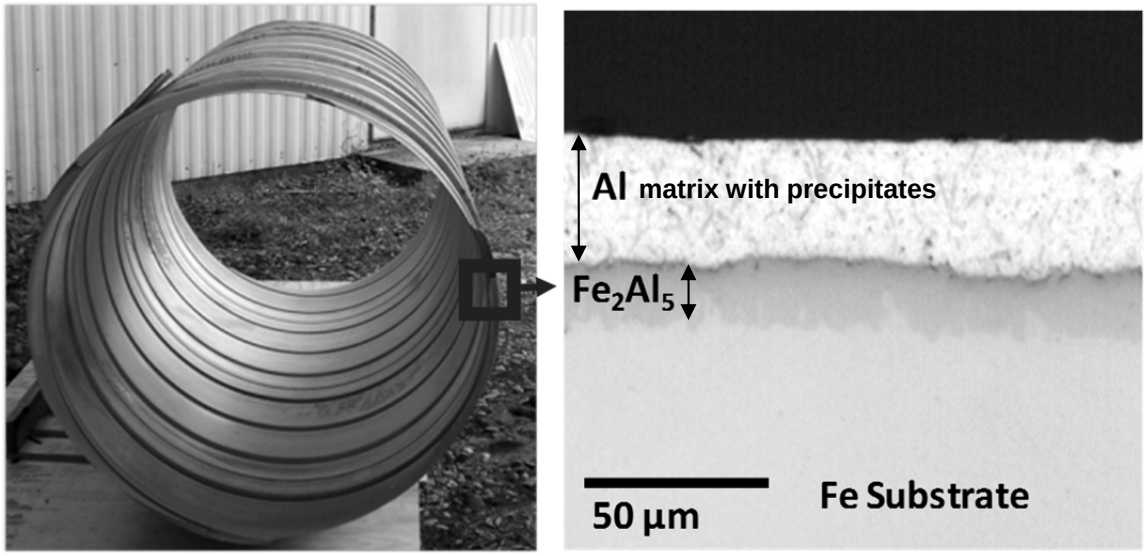

Figure 1 : Metallographic cross-section of aluminized steel

The aluminum coating provides corrosion protection through low corrosion rate of aluminum in mild environment where aluminum is passive, and also may provide galvanic protection to underlying steel under more aggressive environment where aluminum is active (Kimoto, 1999). For that reason, aluminized steel Type 2 is increasingly used for metallic drainage components in contact with natural waters.

Aluminized pipes are commonly ribbed or corrugated for structural strength. Ribbed pipes have better hydraulic efficiency and are often preferred. In the general process (ASTM A760 (ASTM 2010)) used to form spiral ribbed aluminized pipes (SRAP) the stock aluminized sheet is rolled over a series of press dies while lubricated with a soapy solution to decrease friction (Figure 2A). Such construction creates open type ribs as shown in Figure 2B. Interlocking folds are formed in the opposite side of the sheet. As the pipe is rolled into the spiral (Figure 2C), the interlocking fold connects with a corresponding fold on the rib. These formed, not-welded interlocks are called lock-seams and join the segments of spiral pipes.

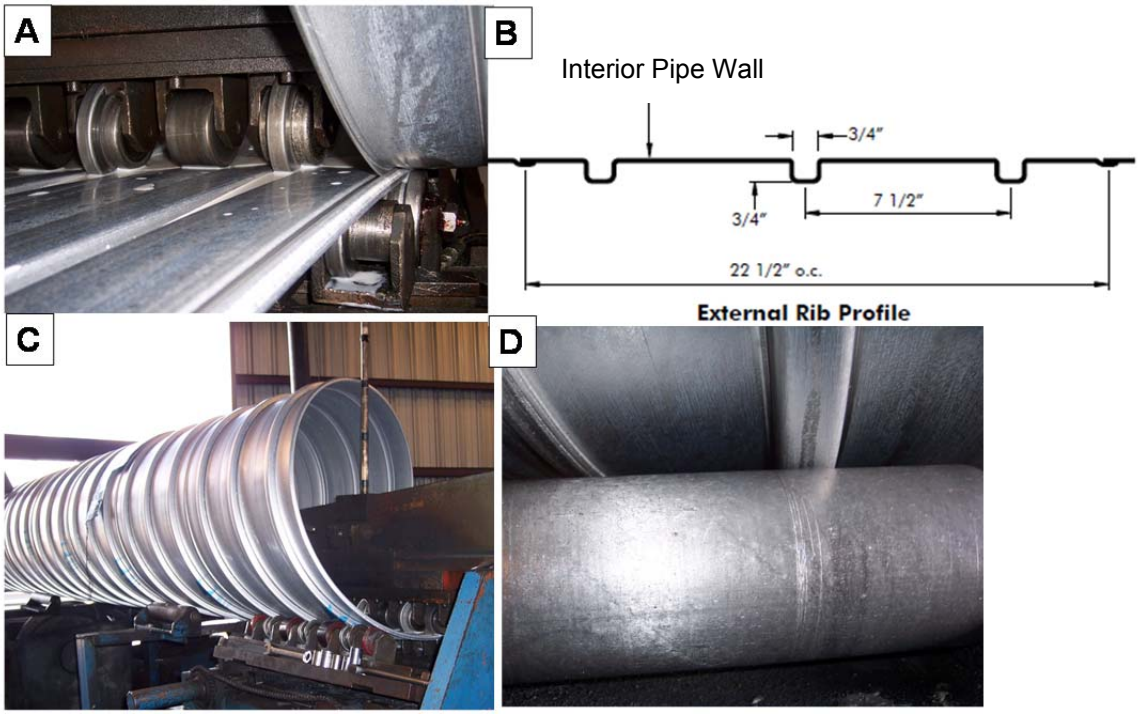

Figure 2: SRAP manufacturing process (A-C); Minor scratches during fabrication of SRAP (D). [Photographs by the Author]

Typically aluminized steel pipes have shown good durability and are expected to have long service life, e.g., 75 years. Previous work by Cerlanek and Powers (Cerlanek and Powers, 1993) estimated that aluminized steel exceeded the service of galvanized steel pipes by two to six times. That advantage of aluminized steel over galvanized steel in part reflects that in galvanized steel the zinc coating is subject to continuous corrosion to provide protection, while in aluminized steel corrosion resistance is provided mainly by a thermodynamically stable thin passive film of aluminum oxide. If this film is damaged or removed by abrasion, another layer of oxide is expected to form rapidly and prevent further corrosion. A detailed review of earlier evidence for aluminized durability has been presented in the previous report on this issue (Sagüés 2009). Based on those expectations and on the prior evidence of good performance, SRAP have been widely specified and used by the Florida Department of Transportation (FDOT) for drainage of runoff water.

1.1.2 Recent Corrosion Failures

Confidence on the long term durability of SRAP has been challenged by recent unexpected early corrosion failures of SRAP installed in various Florida locations. These failures, listed in Table 1, involved severe corrosion and motivated initial research (Sagüés et al., 2009) as well as the continuation investigation reported here.

Table 1: Field failures

Name	Location	Date Reported	Date Installed	Full Penetration	Mode
City of St. Cloud	Indiana Ave.	2005	~2003	Yes	A
City of Largo	West Bay/6th St	2005	~2003	Yes	A
Pasco County	SR-54 & US-19	2006	2001	No	A
Curlew Road, Clearwater	SR 586	2007	1997	Yes	A
Jacksonville	SR 212	2009	2006	Yes	B

In the first (Mode A) much of the corrosion occurred along formed ribs and often also extended into the intervening smooth regions (Figure 3 A and Figure 4). This mode was first reported in 2005 for the drainage system owned by the city of St. Cloud, FL where severe corrosion was accompanied by roadway depressions. The affected pipes had been installed only about 2 years earlier, around 2003. A similar failure was reported also in 2005 for drainage pipes owned by the city of Largo, FL (Figure 3). These pipes were also installed in 2003. At some locations in both sites, the failure was clearly due to mechanical damage during either manufacturing or installation of the pipes (Figure 3B).

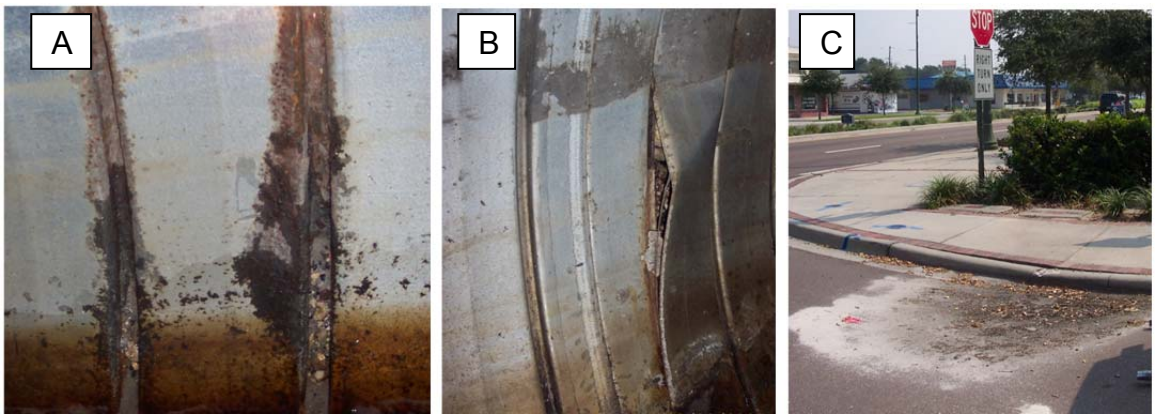

Figure 3: Premature failure of installed SRAP after 2 years in service at City of Largo, FL. (A: Corrosion initiation at ribs; B: Failure due to mechanical damage; C: Road depression due the pipe failure). Photographs by Leonardo L. Cáseres

In 2006, pipe inspections at an FDOT project site at SR-54 & US-19 in Pasco County revealed severe corrosion (but not full penetration) of aluminized pipes installed five years earlier in 2001. Failures comparable to those seen in St. Cloud, were reported in 2007 for a 10 years old installation at SR 586, Curlew Road in Clearwater, FL (Figure 4).

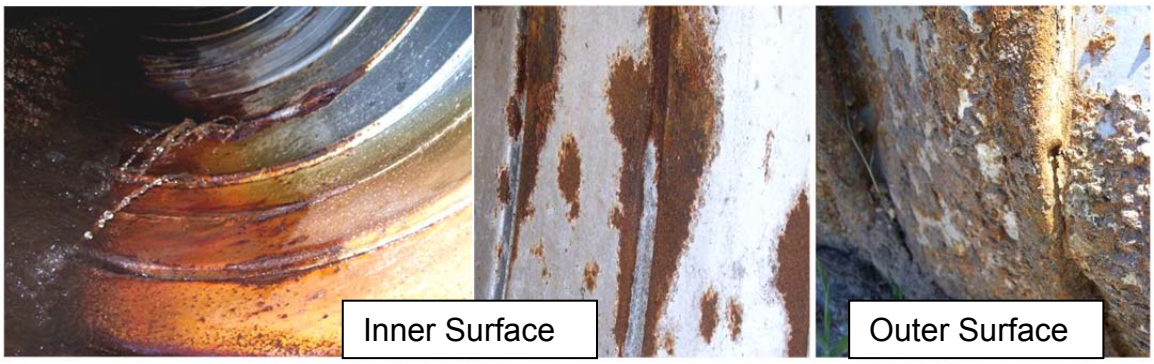

Figure 4: Premature failure of installed SRAP after 10 years in service (From Curlew installation at SR 586, Clearwater, FL)

The second mode (Mode B) of severe SRAP corrosion failure has been documented so far in one location, SR 212 in Jacksonville, Florida, and was revealed in 2009 by video inspection of the installed pipes. The pipes had been in service for only three years. The corrosion was in the form of multiple localized pipe wall penetrations, starting from the soil side, over a > 10 m long section of pipe that was placed on a limestone backfill. The penetrations started from the soil side and did not preferentially affect the ribs.

1.1.3 Understanding of Corrosion Causes and Open Issues

Mode A corrosion was investigated extensively in the field by both the pipe manufacturer and FDOT, and by follow-up initial FDOT-sponsored laboratory studies (Sagüés et al., 2009). It was concluded that much of the corrosion originated from unusual fabrication damage and equipment problems such as stuck rollers. The fabrication damage caused helical cuts along some of the ribs with consequent corrosion loss in those regions. However, not all of the corrosion observed in the field could be explained as being related to severe distress from manufacturing deficiencies. The large localized plastic strain exerted during the mechanical deformation, essential for forming the ribs in SRAP, was considered to have also played a role in promoting or aggravating corrosion. Initial evidence for that mechanism was presented in the report for the previous Project BD497 investigation (Sagüés et al., 2009).

Initial experiments conducted in the previous investigation showed that even moderate amounts of plastic strain cause cracking of the inner layer of the aluminized coating on the steel (Sagüés et al., 2009; Akhoondan et al., 2008). That layer, since it is made up of a brittle Al-Fe intermetallic alloy, cracks readily under tensile stresses such as those encountered during forming. The outer layer, more ductile, can stretch plastically to cover the gaps left by the inner layer cracks. However, if the deformation is large enough, the outer layer fails too leaving underlying steel directly exposed to water and subject to corrosion. The

evidence from the previous laboratory tests and field observations suggests that regular production SRAP in mild service environments has some propensity for localized corrosion at the ribs because of the presence of occasional coating breaks inherent to the corrosion process. If those are the only coating breaks and also are small in size or number, the mild galvanic protection from the surrounding aluminized steel may be sufficient to prevent the onset, or arrest the development, of corrosion of any exposed steel. However, that protection may not be enough under some conditions which are exemplified by, but are not limited to, the following:

1. Large coating breaks, e.g., due to manufacturing defects that introduced cuts such as those observed in the field sites experiencing severe corrosion.

2. Small but numerous enough coating breaks, e.g., produced under still normal but borderline mechanical forming distress.

3. Insufficient galvanic coupling between the exposed steel and the unblemished aluminized surface, e.g., in cases where the environmental resistivity is high and the galvanic macrocell extends to only a short distance away from the exposed steel zones.

4. Excessive anodic polarizability of the unblemished aluminized surface, e.g., when the environment is not aggressive enough to induce appreciable localized passivity breakdown or passive film dissolution of the aluminum film, so galvanic action is negligible.

Under conditions such as those, the corrosion of steel exposed at the breaks may proceed unimpeded, with possible penetration of the culvert wall by Mode A corrosion after a period of only a few years. The process could be aggravated by the development of rust crests at the corroding spots, which may provide sites for additional local cell cathodic reaction (likely O_2 reduction) with elevation of the mixed potential and consequent increase of the steel corrosion rate. Further aggravation could result from sacrificial consumption of the aluminum near the edge of the corroding steel, perhaps enhanced by the

production of hydroxide ions from oxygen reduction as indicated in Sagüés et al. (2009). The aluminum consumption near the edge could in turn expose additional steel there resulting in propagation of a corrosion front starting from the initial blemish. Such mechanism could explain the observation of corrosion propagating away from the initial distressed ribs in the early corrosion field incidents (Sagüés et al., 2009). Elucidation of the factors noted above was necessary and was addressed by the investigation reported here.

Mode B corrosion was not uncovered until after the completion of the previous study, Project BD497. Because the deterioration took place with SRAP on limestone backfill, it was speculated that the corrosion was due to rapid wastage of the aluminized layer in a high pH medium created by interaction of groundwater with the limestone. That hypothesis and its consequences on the selection of backfill materials for SRAP, as well as possible synergism between both modes of corrosion, were also examined in this investigation.

1.2 Project Objectives and Research Scope

The issues introduced in the previous section defined the objectives of the work reported here, stated as follows:

- Establish to what extent the Mode A corrosion incidents can be ascribed to manufacturing defects that can be rectified by appropriate quality control, as opposed to an intrinsic vulnerability to corrosion of regularly produced SRAP due to ordinary forming strains.

- Determine the mechanism responsible for Mode B corrosion and the role that limestone backfill played in that deterioration.

To address those objectives, the scope of activities was organized along the following thrusts that are keyed to the following sections of this report:

Assess field evidence by detailed analysis of the Mode B site case and of potentially related sites.

Assess mechanical distress in SRAP ribs in coupons from Mode A corrosion field locations and from regular production pipe as well as intentionally formed aluminized steel. Identify possible correlations between mechanical distress and corrosion in the field.

Formulation of test solutions for simulating natural waters in corrosion tests.

Effect of mechanical distress on corrosion performance of aluminized steel in simulated natural waters. In this major area of the investigation, experiments addressed comparative performance of flat and severely deformed aluminized steel stock; SRAP and ordinary corrugated aluminized pipe samples in both stagnant and moving waters; and effect of simulated severe manufacturing distress (exposed cut edges).

Determine mechanism of corrosion in water contacting limestone. This other major area of the work involves comparative corrosion experiments in clean sand and in limestone, including the effect of water flow in the latter.

Conduct a general discussion of the project findings. The findings from the previous thrusts are discussed in the context of mechanism responsible for SRAP deterioration.

2. FIELD EVIDENCE

The Jacksonville SR 212 failure (Mode B) was investigated by Rodney G. Powers & Associates for Contech Construction Products, Inc and the results were reported to FDOT in November 2010. According to this report (CONCORR Florida, 2007) the pipe line was located ~ 8-12' below pavement. Water inside the pipe had a depth approximately 10" and was pumped down to approximately 4" for testing; significant ingress of water through holes in pipe invert occurred due to existing head pressure. Approximately 1 to 2" sand in invert was observed. The presence of crushed limestone in the pipe surroundings was discovered. Four coupons were extracted from the site of which one was made available to the University of South Florida for examination. Metallographic cross-section of this coupon was prepared according to procedures explained in previous report chapter 5 (Sagüés et al., 2009). This coupon was further investigated using scanning electron microscopy (SEM) and energy dispersive spectroscopy (EDS).

Severe localized corrosion took place starting from the soil side, on the smooth inter-rib regions of the culvert pipe, in contrast to the type of damage observed in the Mode A incidents. The corrosion took place on a > 10 m long section of the pipe and involved multiple perforations typically ~ < 1.5 cm diameter. The cross-section metallography of the soil side revealed that although the outer aluminum coating was almost deteriorated completely, the intermetallic layer seemed to stay nearly intact. Only minor coating attack was observed on the water side.

While stray currents or microbiological activity cannot be completely ruled out as the possible causes of this incident, special attention was given to the chemical effect of backfill material due to potentially high pH at the surrounding water and soil due to the use of limestone. Figure 5 illustrates the location of the

bore [top left], extracted coupon [top right] and metallographic cross-section of the coupon [bottom].

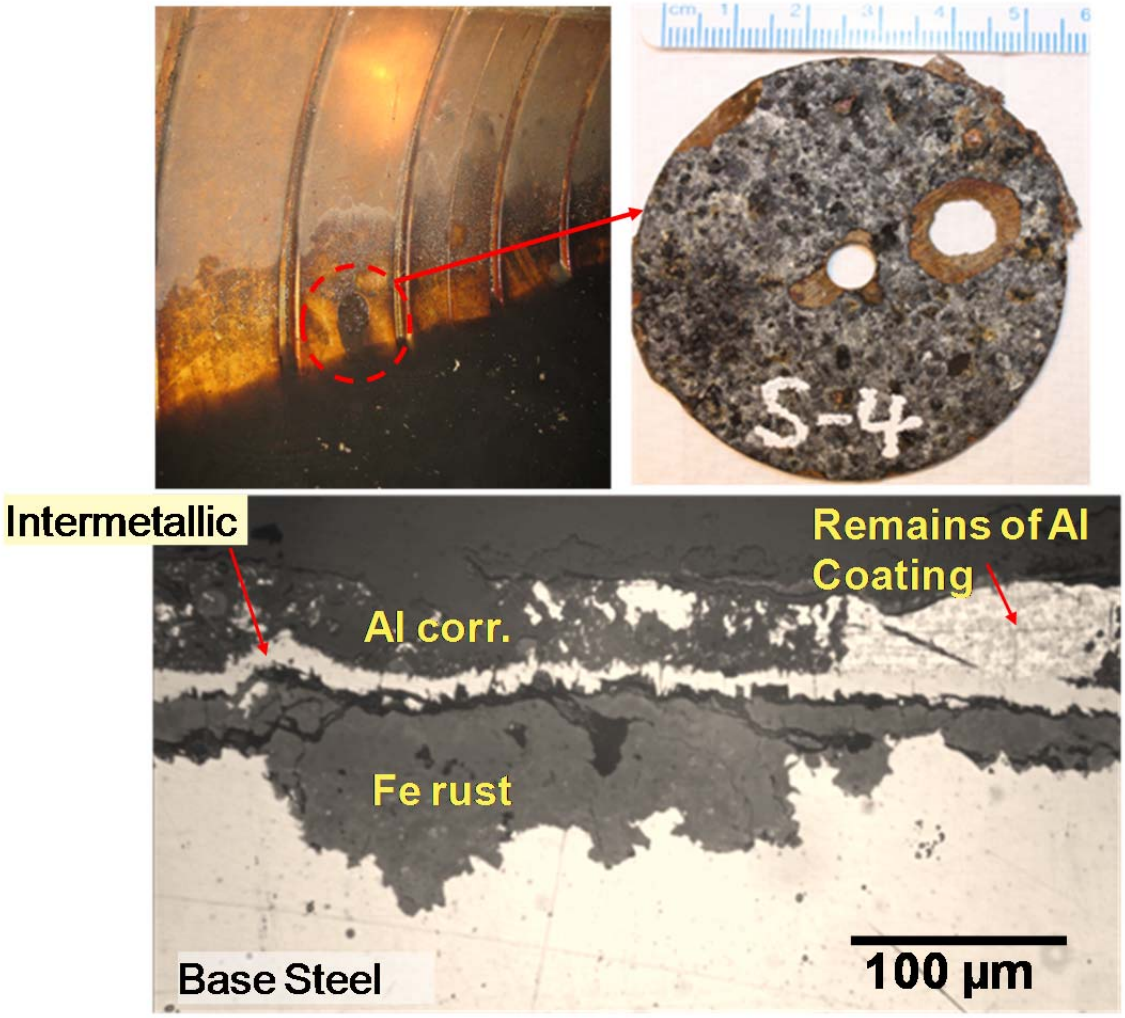

Figure 5 : Location of the bore [top left], extracted coupon [top right] and metallographic cross-section of the coupon [bottom].

Another field trip on March 3, 2011 was coordinated between the University of South Florida and FDOT for inspection of SRAP at a site that was near the failure just described and that may have had a similar soil environment. Although due to hazardous conditions entering the pipe was not possible, several potential measurements were made with the help of the diver inside the pipe. The potentials measurements were typically around -.580 mV vs. saturated

calomel electrode (SCE) agreeing with previous measurements reported for the aluminized pipes in service (Federal Highway Administration, 2000) and not indicative of unusual circumstances. Also, water samples were collected and tested for conductivity and pH. Neutral pH values of 7-8 were observed for the water samples. Due to flooding, no soil samples suitable for identification of materials in the backfill could be collected. A pipe coupon obtained at a 10 o'clock orientation did not show signs of corrosion at either side, either visually (Figure 6) or upon metallographic examination. Hence, despite the proximity to the other failure site, corrosion damage was not detected at this location.

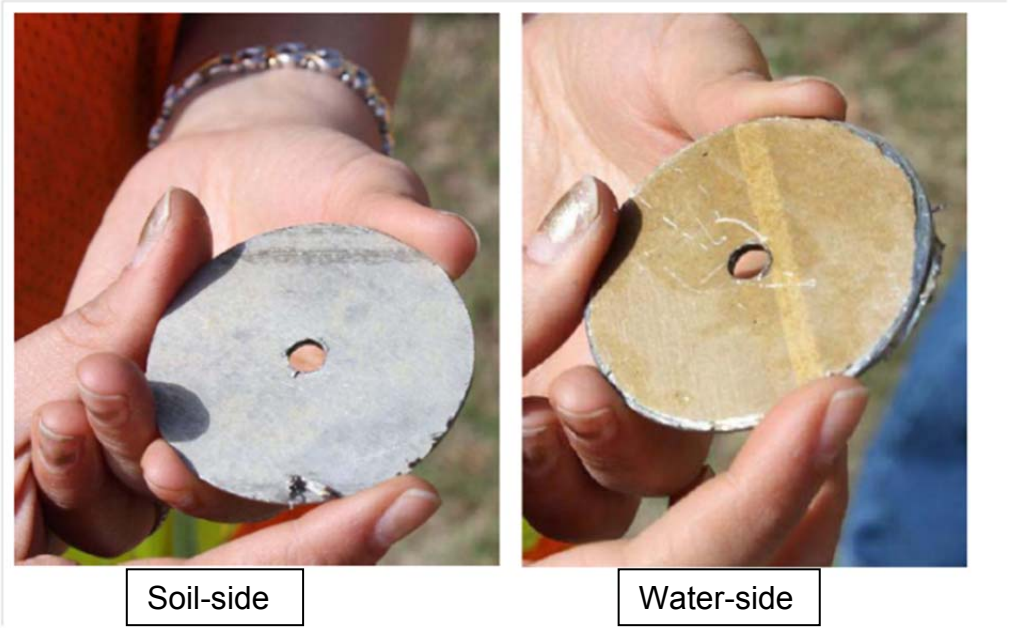

Figure 6 : The pipe coupon from a site that was near SR 212 failure [at Wolf Creek/Beach Blvd] did not show signs of corrosion at either side.

A third field inspection took place on February 23, 2012 for another SRAP site in the general proximity of the site of the first failure, near the Highland Glen and Beach Blvd intersection in Jacksonville, following reports of a pipe failure. Significant mechanical deformation and ripped sections indicative of partial collapse were observed at the entrance of the pipe, as shown in Figure 7. Some corrosion products were observed around these stressed regions. Also, corrosion

was observed in plain corrugated galvanized pipe segments that were used to join sections of SRAP.

Figure 7: Photograph of in-situ pipe located in Jacksonville, near Highland Glen and Beach Blvd. Mechanical damage (top left, bottom), Limestone rocks present beneath the bore location (top right).

Excluding the mechanical damage, it appeared that the rest of the SRAP section inspected was generally in a good condition and was not significantly corroded. The water samples pH and conductivity were about 6.3 and 2 kΩ-cm, respectively. The soil sample (mud taken from underneath the extracted field coupon) pH and conductivity were about 7 and 7 kΩ-cm, respectively. These values are within the range of accepted design environments for SRAP and did not appear to have been initiators of the observed deterioration. Some limestone rock was revealed beneath of core sample hole. Unfortunately the pipe specimen however could not be retrieved due to adverse site conditions. Based on the overall observations, the failure appears to have been of structural/mechanical origin and the associated corrosion reflected only the widespread exposure of base steel at cuts and rips.

3. MECHANICAL DISTRESS IN SRAP RIBS

As indicated in the introduction, it was important to compare mechanical strain in newly produced pipe to the strain present in coupons extracted from pipe affected by Mode A corrosion. In particular, it was desired to determine if the radius of curvature at the rib bends in the older pipe was significantly smaller (indicating greater plastic strain) than that in newly produced pipe. If such greater forming severity was observed, it could be interpreted as having been a contributing factor to the observed corrosion. The newly produced pipe was made following awareness of the previous corrosion incidents, and is assumed to reflect adherence to high quality manufacturing practice.

An initial assessment of this issue was conducted as part of the previous investigation (Sagüés et al., 2009), using a portion of an extracted pipe which failed prematurely by corrosion at the Curlew Road site (Table 1). The pipe portion contained corroded regions but for these tests the ribs were sectioned at spots that had not showed significant corrosion, so accurately dimensional measurements could be made. The outer (tension side) and inner (compression side) radii of curvature of the bends was measured in four different cross-sections. Each cross-section yielded eight radius measurements (Figure 8 shows a schematic with the circle fit for each) for a total of 32 values. A similar sampling took place for five cross-sections from a newly produced pipe from the same ("1st") manufacturer as that for the pipe used in the Curlew site, produced under strict quality control. For this project, newly produced pipe from another ("2nd") manufacturer was similarly analyzed. The results for the three samplings are plotted in Figure 8 as cumulative distributions. The solid lines show cumulative normal distribution fit lines for the data in each case.

The results in Figure 8 show differences between the average radius of the various cases that are in the order of, or less than the corresponding standard deviations. Moreover, the average radius for the Mode A corrosion case

fell in between those of the samples from the two manufacturers. Overall, the results do not support the hypothesis that the Mode A corrosion was associated with earlier pipe production having experienced unusually severe fabrication forming, at least as measured by the value of the radius of curvature at the bends.

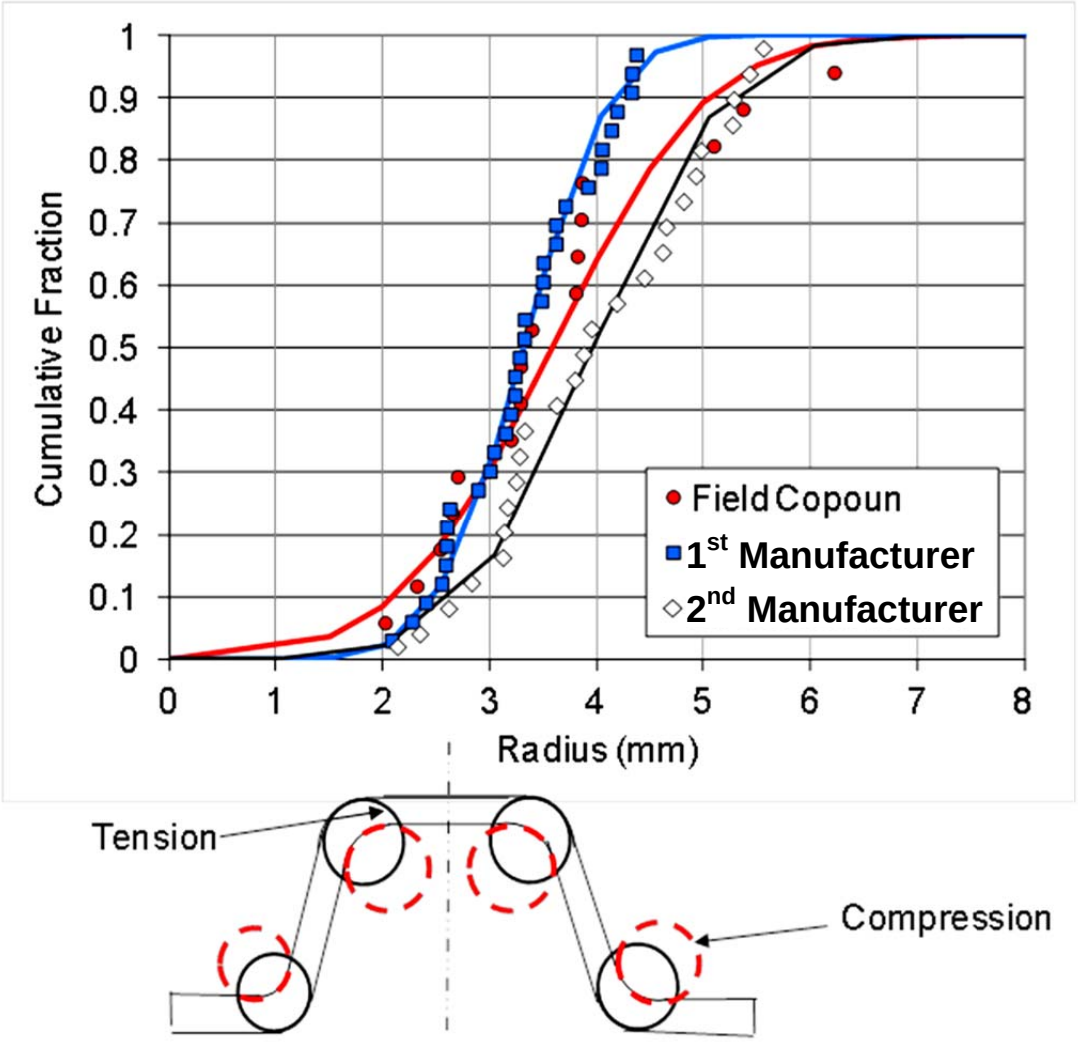

Figure 8 : Comparison of cumulative distributions of rib radius of curvature (mm) between samples from newly produced aluminized steel type 2 pipes made in two different manufacturers and from a pipe once in service for 10 years at the Curlew Rd. site. The schematic shows the position of the circles fit to each bend for each cross-section.

To further correlate the coating damage to the extent of metal forming, tensile tests were performed on specimens made of gauge 16 flat aluminized steel sheet, with a 0.5 inch wide and 4 inch long central section (Figure 9). Except for a short necked region which experienced ~50% strain, the rest of the central section experienced ~20% strain with minimal outer coating break. This strain value was comparable to the value calculated for SRAP at the ribbed regions using the change in metal sheet thickness at the formed region. However, breaks in outer aluminum coating at the ribbed regions are common. Figure 10, illustrates the surface cracks observed by SEM at the tension side of the bend as well as the typical metallographic cross-section of bend areas. Therefore, it was speculated that the generation of breaks in outer aluminum coating in SRAP is mostly due to bending as opposed by stretching of the sheet metal by the rollers during rib forming process.

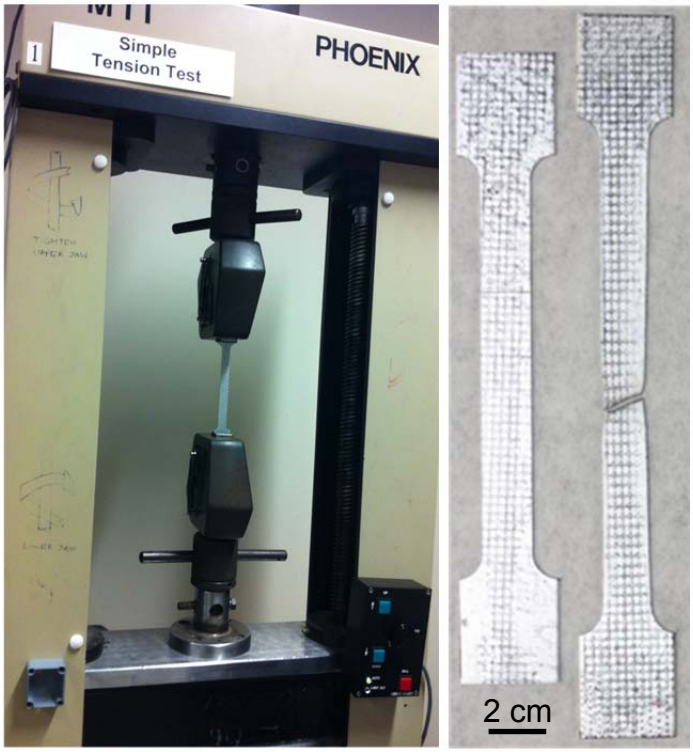

Figure 9: specimens before and after tensile test.

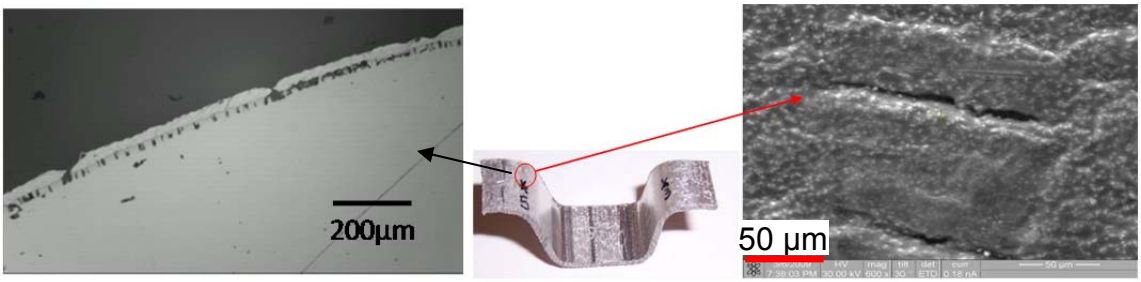

Figure 10 : SEM image of the bend at rib regions of newly produced SRAP (right), Metallographic cross-section of bend region (left)

Figure 11, illustrate the tensile specimens and their metallographic cross-section near by the necking zone. While significant amount of breaks occurred in the intermetallic very few outer coating breaks were present. To see direct occurrence of corrosion at regions with coating breaks, parts the tensile specimens were immersed in solution S after the edges were covered with epoxy. As shown in Figure 12 at a very small length near the necking zone the corrosion products in forms of yellow shade are present. The control specimen with no stress shows no sign of corrosion after few days of exposure.

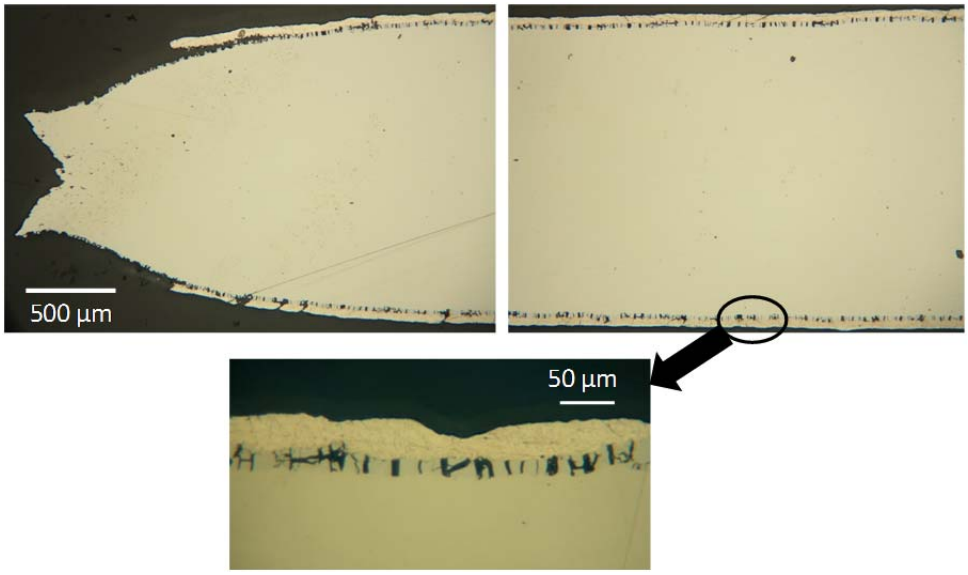

Figure 11: Metallographic cross-section of tensile test at the necking zone (top left) and ~1 cm away from the necking zone (top right)

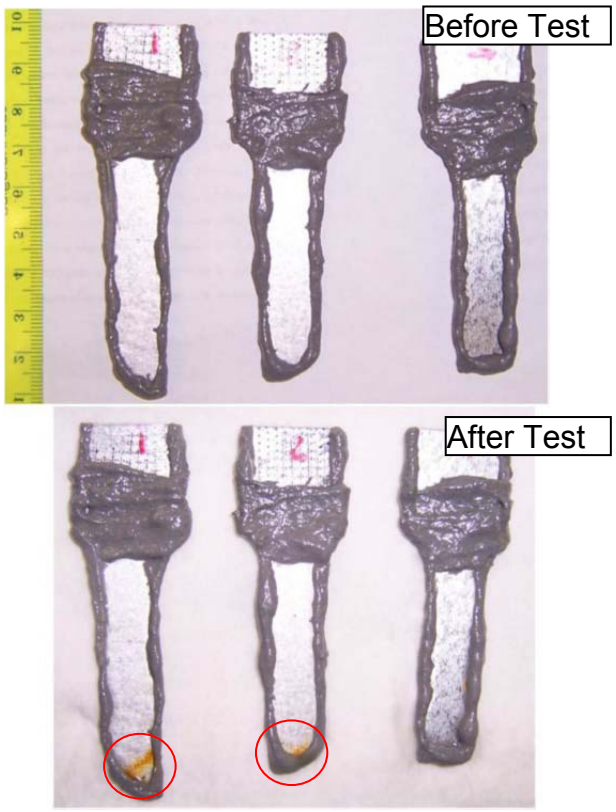

Figure 12: Tensile specimens before (Top) and after few days of immersed in simulated natural waters (Bottom). Minor corrosion signs appeared at a short distance from the necking zone. The control specimen (far right) doesn't show signs of corrosion.

4. FORMULATION OF TESTS SOLUTIONS

4.1 Specifications on Environmental Limits

Understanding the current FDOT selection and installation guidelines, as well as assessing the water and soil/backfill samples from the field, is vital to replicate the typical field condition in the laboratory. General guidelines were discussed in the previous report (Sagüés et al., 2009). Below is a brief summary of these general guidelines in addition to more specifics regarding the backfill materials properties.

FDOT recognizes four governing environmental parameters that have direct effect on service life durability of pipes. These parameters are pH, resistivity, and chloride and sulfate ion concentration. Therefore, before selecting any type of pipe, environmental tests should be conducted to measure these elements. FDOT developed a computerized culvert service life estimator software to help with material selection and determination of minimum wall thickness for a given design service lifetime (Cerlanek and Powers, 1993). For metal culvert piping, the time of first perforation (complete penetration) is considered to be the service life end point. An FDOT chart for estimating years to perforation of 16-gauge aluminized steel Type 2 culvert pipes is reproduced in Figure 13.

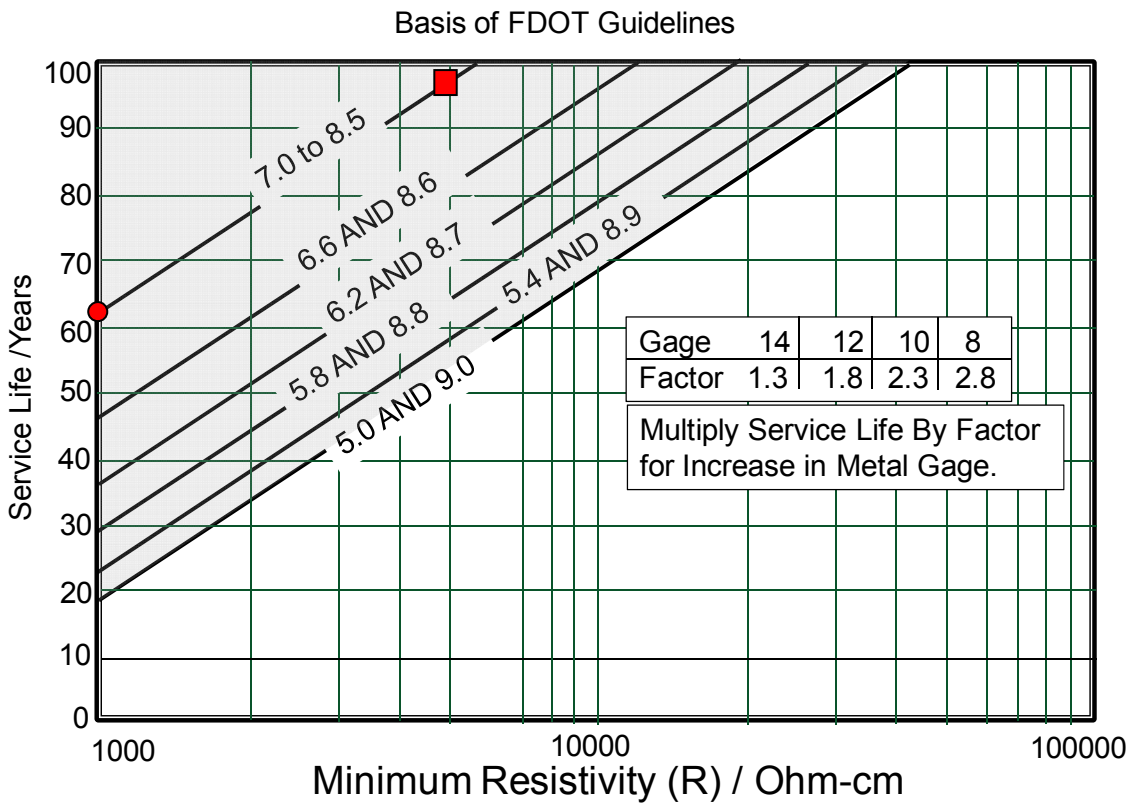

Figure 13: The FDOT chart for estimation years to perforation of 16-gauge aluminized steel Type 2 culvert pipes (solid lines) (Cerlanek and Powers 1993). Light shade triangle illustrates the service life functionality envelope. The circle and the square indicate the conditions for Solution S+ and S, respectively.

Once the pipe is selected and excavation conducted typically the original soil excavated from the site is used as backfill material. However, if the pipe is below the water table and the dirt excavated is unworkable (e.g., extremely wet or has high organic content) then according to FDOT specification 12-8.1.3, the engineer may decide to use backfill materials obtained from a different source. In this case, construction aggregates complying with ASTM C568-96 may be used for bedding and backfill of pipes to provide good structural support. As of the beginning of this investigation, limestone was allowable for that purpose.

Pipe bedding and backfilling materials may have a significant effect on the corrosion performance of pipe by changing the pH of pipe's surroundings. FDOT

design drainage handbook (FDOT, 2008), states that the environmental tests should also be performed on structural backfill material or any subsurface materials along drainage alignment. In fact, the issue of testing backfill material is also pointed out in FDOT soil and Foundation Handbook section 4.10. However, many times FDOT uses the general term “environment condition” to describe the properties of soil and water in immediate contact of the pipe; this may lead to misinterpretation of this term describing only the properties of original soil before pipe installation and not those of backfill imported from a different site. Therefore, the possibility of applying aggressive backfill materials based on availability exists. Materials such as crushed concrete, typically used as backfill material for other constructions, is extremely aggressive to aluminum coating as they cause the elevation of pH to unacceptable values .

Other physical requirements for culvert pipe backfill are described in Florida Specification 125-8.3. In this case the trenches for the pipes are split into 4 separate zones shown in Figure 14.

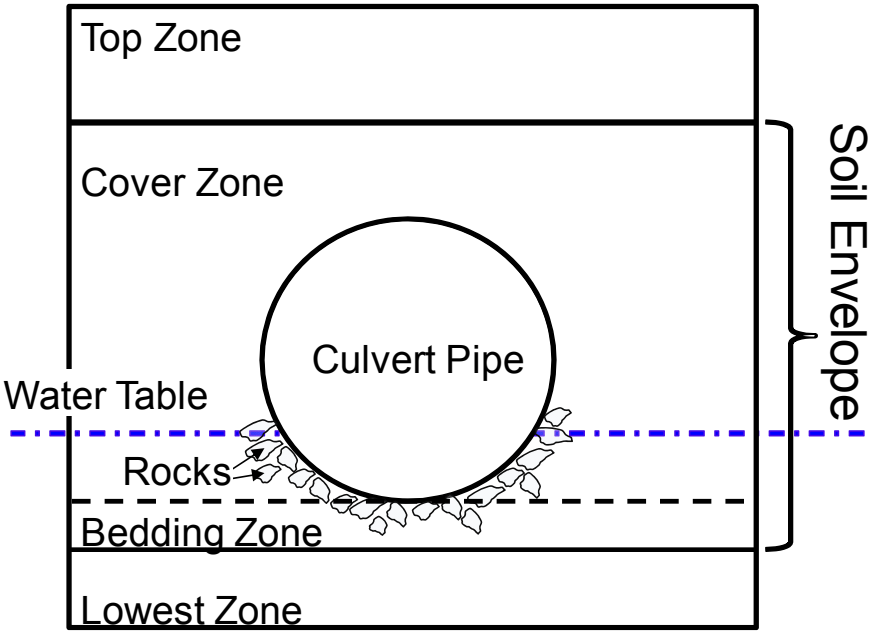

Figure 14: Typical Pipe Layout

4.2 Replication of Field Conditions

To simulate field conditions within the range specified by FDOT, typical Florida water/soil properties were considered. In a previous study (Cáseres, 2007), water and soil samples from several Florida locations were analyzed to obtain the typical concentrations of chloride and sulfate ions present near currently installed aluminized pipes. Typical water hardness, alkalinity and resistivity were also obtained. These data were evaluated and considered in generating a solution replicate of actual field conditions for this investigation. As a result, two simulated waters of S and S+ with the following properties were chosen for laboratory testing. Solution S properties were detailed in previous report (Sagüés et al., 2009) and are repeated below.

Solution S (already used in the FDOT Project BD497 investigation, (Sagüés et al., 2009)) has pH ~ 7, chloride and sulfate concentrations of 34 and 30 ppm, respectively. While not having a high precipitating tendency, this solution is considered as relatively benign due to small content of aggressive ions (chloride and sulfate) and high resistivity ~ 5000 Ω-cm. Under current FDOT design guidelines for highway drainage culverts, a service life of ~100 years could be expected (Cerlanek and Powers, 1993) for this condition.

Solution S+ has pH and sulfate concentration similar to Solution S but a significantly larger amount of chloride (230 ppm) with consequently lower resistivity (~ 1000 Ω-cm). This solution is therefore more aggressive. A service life of less than 65 years could be expected (Cerlanek and Powers, 1993).

Although above solutions may well represent the typical soil/water conditions in Florida locations, they may not represent the properties of backfill materials commonly used in the installation of culvert pipes. In order to replicate typical backfill conditions and based on the recent failures prescribed to the use of limestone backfill, a series of experiments fully discussed in chapter 6 were performed.

5. EFFECT OF MECHANICAL DISTRESS ON CORROSION PERFORMANCE OF ALUMINIZED STEEL

This major focus of the investigation is the laboratory evaluation of corrosion performance of aluminized steel with various extents of coating breaks and mechanical distress exposure to relevant simulated natural waters.

Work conducted under the previous project BD497 (Sagüés et al., 2009) had examined the comparative corrosion evaluation of severely deformed aluminized steel and undeformed, flat stock. Specimens of both types were exposed to solution S. The results showed that aluminized steel strongly formed by spherical indentation was susceptible to early corrosion development. In contrast, undeformed aluminized surfaces showed much less deterioration during the same test interval. It was concluded that solution S was not aggressive enough to induce strong manifestations of localized passivity breakdown or passive film dissolution of the aluminized coating, at least in the short term. Consequently, the aluminized coating would not have provided substantial galvanic protection of the steel substrate under those conditions, resulting in early corrosion of exposed steel in formed regions. Those findings may explain in part why early Mode A corrosion was experienced at the field locations under nominally mild environmental conditions.

In the present investigation, the experiments were expanded to additionally examine:

- The comparative corrosion evaluation of regular production SRAP and less strongly deformed plain corrugated aluminized pipe (PCAP).

- Evaluation of corrosion in aluminized steel with exposed cut edges replicating severe manufacturing distress.

Routine electrochemical measurements such as open circuit potential (E_{OC}), electrochemical impedance spectroscopy (EIS), and cyclic cathodic and anodic potentiodynamic polarization were performed to assess the corrosion behavior of specimens during the time of testing. Solutions' pH and conductivity were also monitored periodically. The specimens were also inspected visually for corrosion development. Metallography, SEM and EDS methods were also used to analyze the depth of corrosion propagation after the exposures were completed.

5.1 Comparative Corrosion Evaluation of Spiral Ribbed and Plain Corrugated Pipes

5.1.1 Preliminary Tests

Following the observations from the previous investigation, further exploratory tests were conducted in which small (e.g., 3 x 3 in) samples of regular production SRAP including the rib deformation were cutout of a newly produced pipe. Control specimens (2 x 3 in) were also cutout from the smooth regions between the ribs. The cut edges were sealed with either beeswax or epoxy. These specimens were exposed to solution S and the more aggressive solution S+ (section 4.2). Figure 15 illustrate the corrosion progression for a ribbed specimen (edges covered with beeswax). Figure 16 shows the average E_{OC} for each category. Ribbed samples showed various instances of visible rust development along the rib bends, with little indication of corrosion slowing down and with potentials that confirmed little galvanic protection from the rest of the aluminized surface. The smooth specimens showed minor pitting, but not significant deterioration indicated. No significant difference was observed in potential measurements or the corrosion progression of the specimens in solution S compared to those of the specimens in the S+ solution.

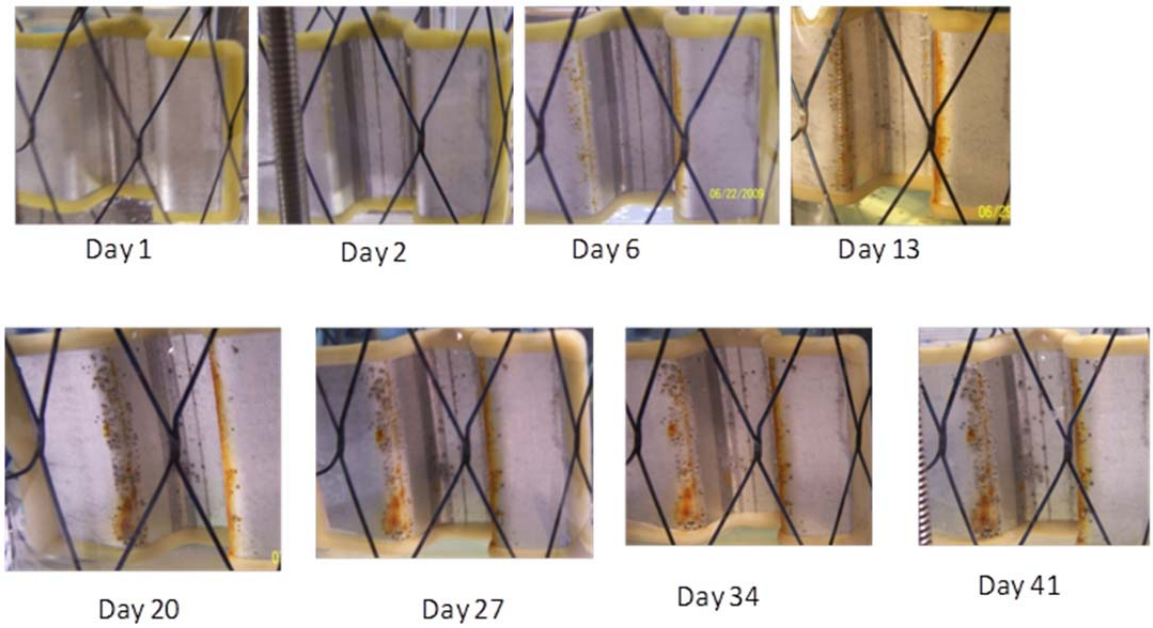

Figure 15 : Corrosion progression of small ribbed specimens in S solution; the ribbed regions show significant pitting while the flat regions look bright.

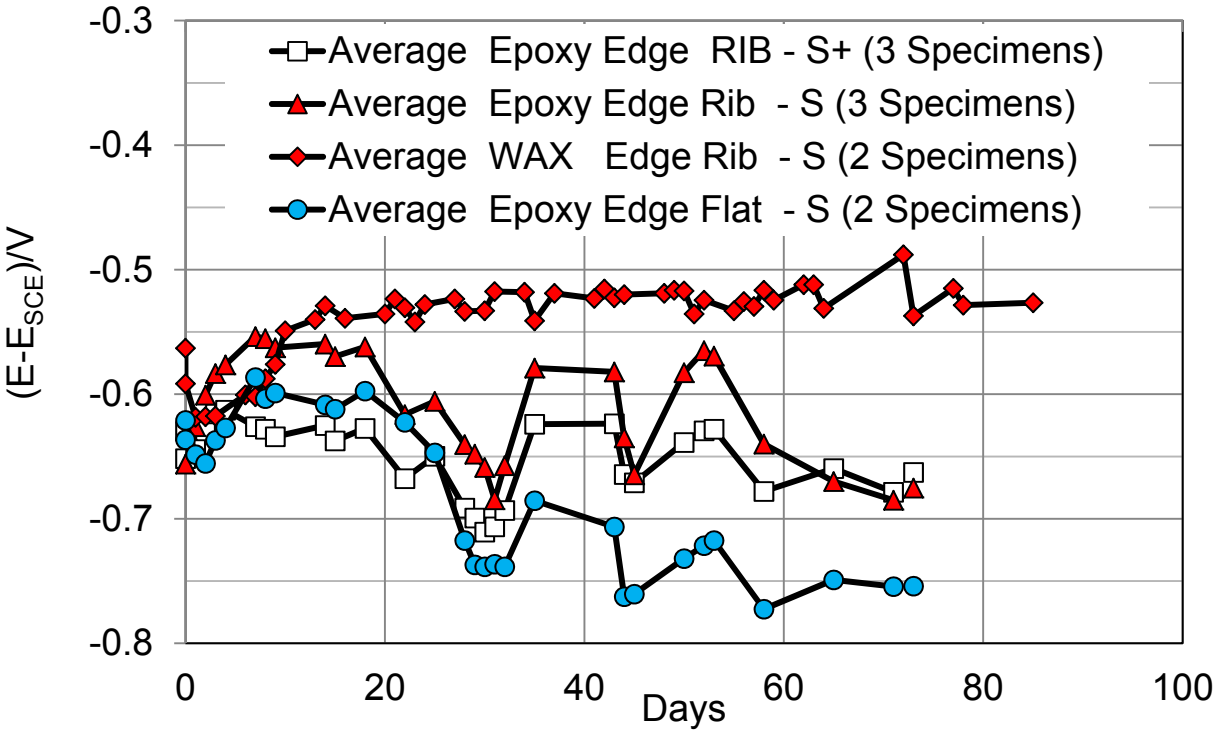

Figure 16: Average E_{OC} for small size SRAP specimens

5.1.2 SRAP vs. PCAP in Non-flowing Waters

Since crevice corrosion (occurring underneath the epoxy), could have obscured the results of previous experiment, a new set of experiments was launched with much larger specimens. In that case, the ratio of specimen's edge to the total surface area was less significant, reducing the effect of possible crevice corrosion on the corrosion performance of the entire system.

These experiments involved comparative corrosion evaluation of regular production of SRAP and PCAP which were conducted with large pipe coupons (18 x 10 in) in the solutions S and S^+ developed earlier. The solutions in these experiments were not replenished representing the stagnant waters (non-flowing) condition in the pipes. However, the solution level was kept constant by periodic additions to make up for evaporation. Similar electrochemical measurements to those indicated above were taken for this series.

Figure 17 illustrates the typical surface discoloration occurred on both SRAP and PCAP specimens after about two years of exposure. The discoloration occurred below the water line, while the top of specimens above the water line stayed bright. Minor pitting of aluminum occurred after a year of exposure in both solutions. Figure 18 shows the typical appearance of a pit at the rib region after a year of exposure. EDS confirmed the present of aluminum corrosion products at the dark grey regions and iron corrosion products at seams regions.

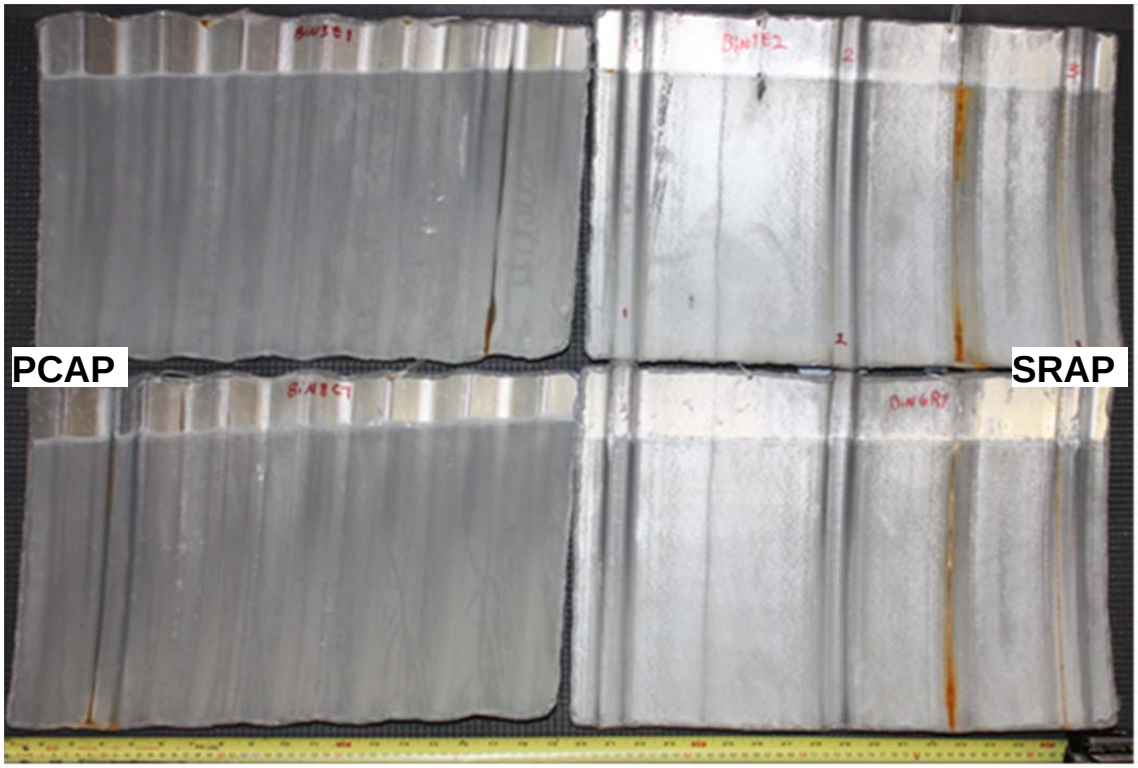

Figure 17 : PCAP and SRAP specimens in S solution [Top] and S^+ solution [Bottom] after ~700 days of exposure.

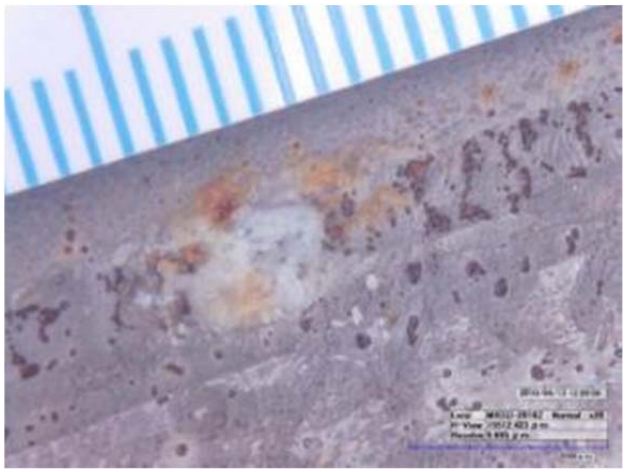

Figure 18 : Pits and corrosion product at ribbed regions of an in-situ SRAP specimen after ~300 days of exposure. 1 mm markers.

Apart from minor pitting and the observed coating discoloration, corrosion was not pronounced. The metallographic cross-section of extracted specimens

was compared to unexposed specimens (Figure 19). Coating loss was observed after two and half years of exposure was insignificant.

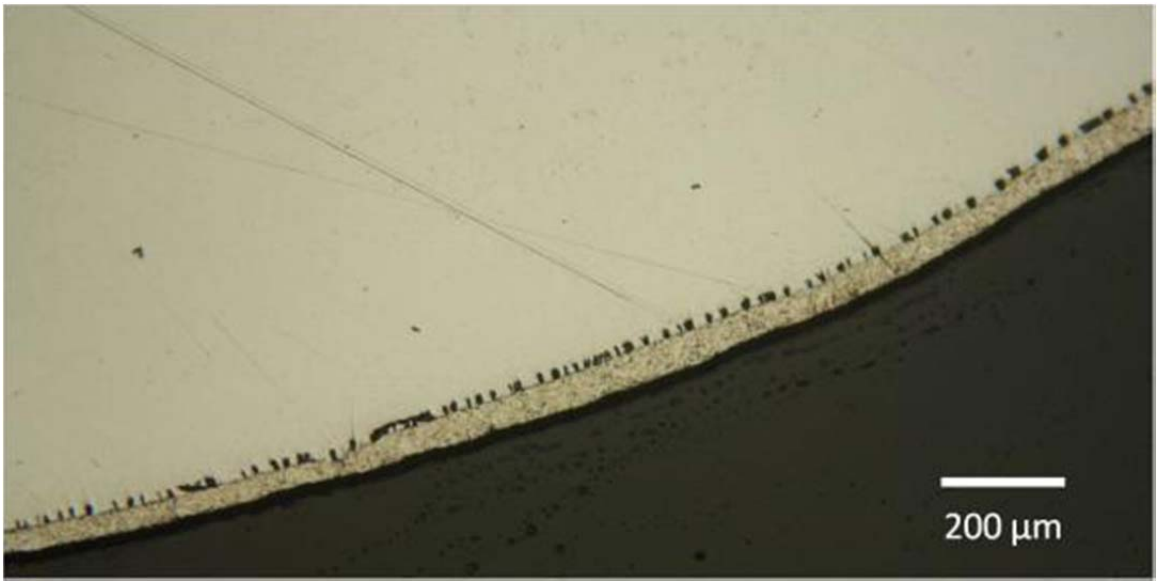

Figure 19 : Metallographic cross-section of SRAP at rib regions after two years of exposure to solution S. No significant coating loss is observed.

EIS measurements also demonstrated extremely low corrosion rates (< 1-2 µm/yr) in both aggressive and nonaggressive solutions indication of reasonable corrosion resistance of aluminized pipes to simulated natural waters.

The E_{OC} (Figure 20) is slightly more positive for SRAP in solution S, where aluminum is mostly passive and the system is polarized due to steel substrate exposed at the formed regions.

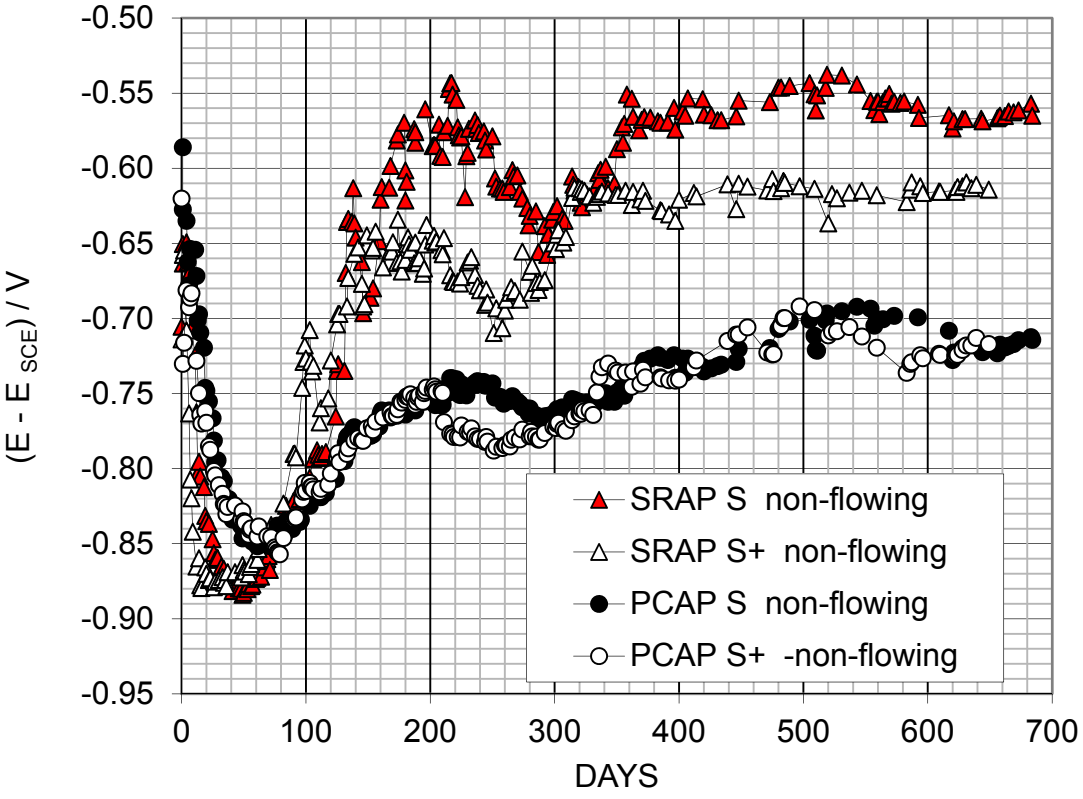

Figure 20 : E_{OC} of SRAP and PCAP in solution S and S+

Figure 21 compares the apparent corrosion current density of two categories of pipes (SRAP and PCAP) in solutions S and S+ . While slightly higher corrosion rates took place for SRAP in aggressive solution, no dramatic difference was observed suggesting no inherent deficiency with normal production of these pipes.

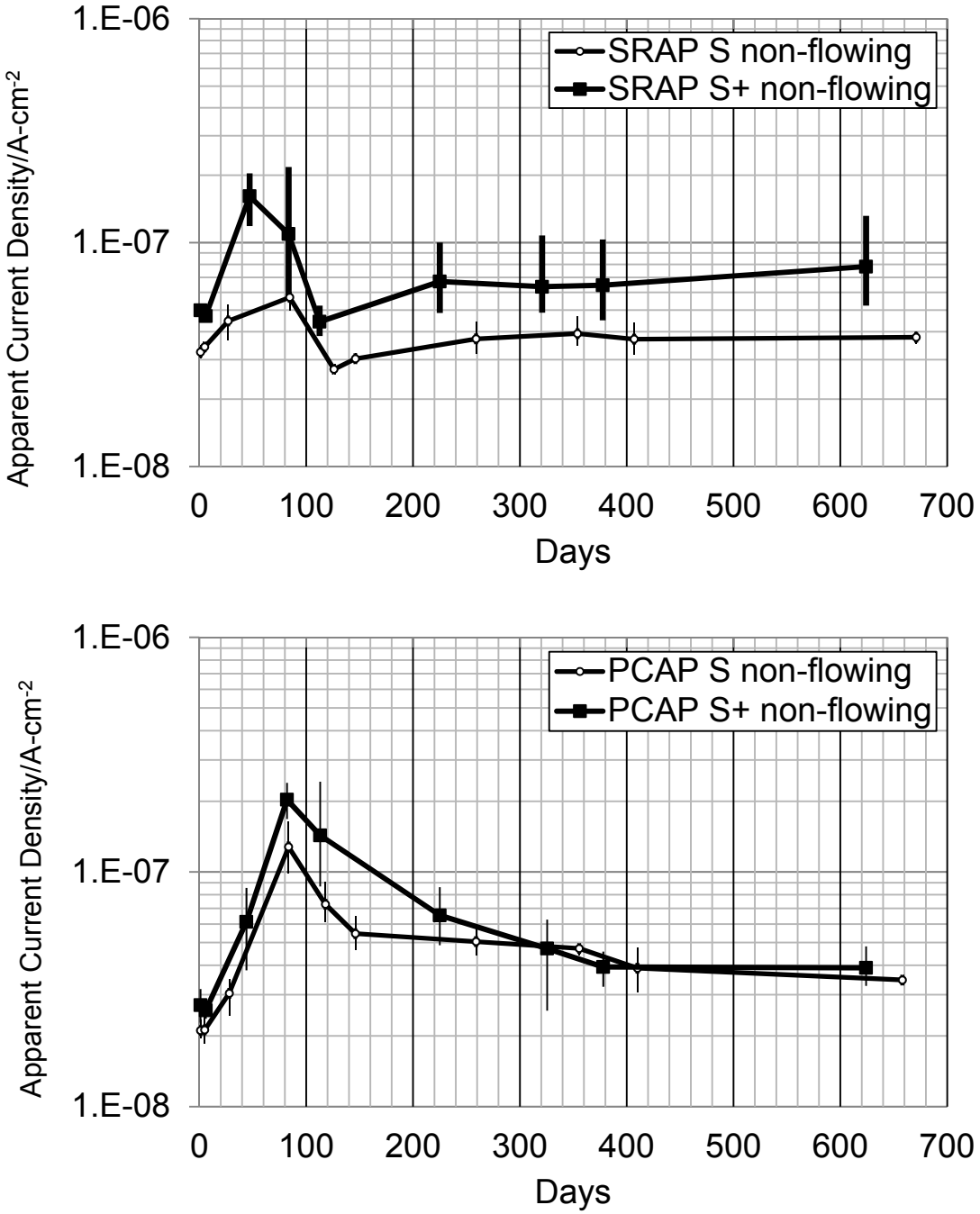

Figure 21: Apparent corrosion current density of SRAP (Top) and PCAP (Bottom) in solution S and S+

It may be argued that the low corrosion rates observed for SRAP and PCAP in these experiments is due to a high concentration of ionic corrosion products in the stagnant waters which may arrest the progression of the corrosion processes. To test such hypothesis, Solution S was renewed for two of the quadruplicate specimens at about ~560 days of exposure. Figure 22 and 23 demonstrate only insignificant change in E_{OC} and corrosion rates after solution renewal, suggesting that the low corrosion rates are not the result of compositional changes in the solutions.

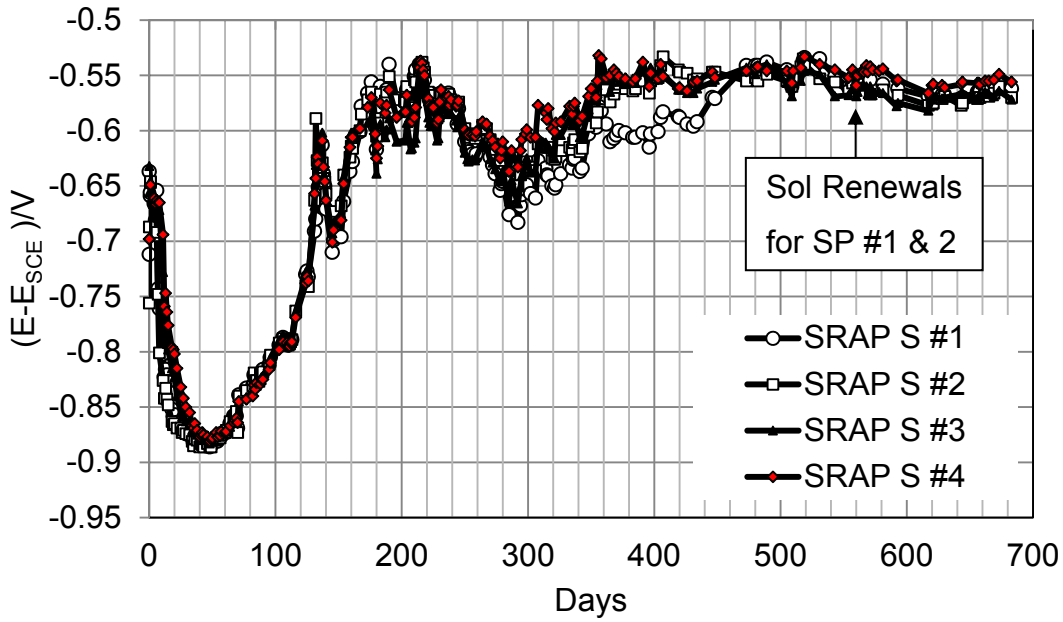

Figure 22: E_{OC} of quadruplicate SRAP specimens in Solution S. Solution was renewed for Specimens 1 and 2 at ~560 days of exposure. No change observed.

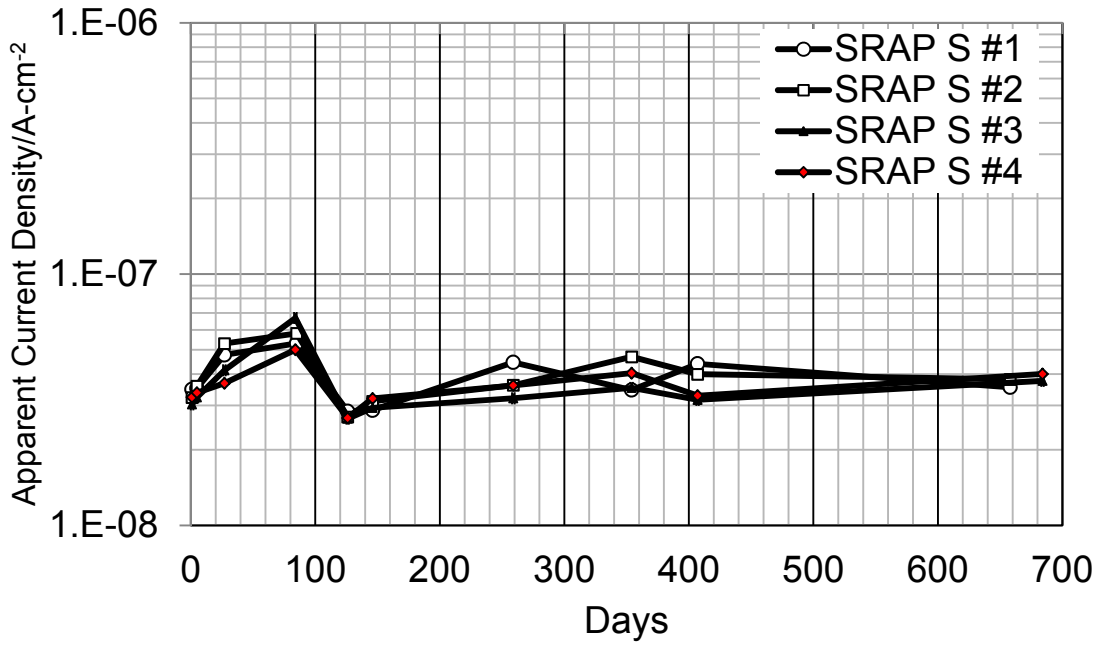

Figure 23: Apparent corrosion current density of quadruplicate SRAP specimens in Solution S. Solution was renewed for Specimens 1 and 2 at ~ 560 days of exposure. No change observed.

5.1.3 SRAP in Flowing Waters

To simulate the condition of the pipe in the rainy season when the water constantly flows in the pipes, a new set of experiments with flowing simulated waters was conducted. It should be noted that abrasion due to flowing water for steep slope pipe installations is a major damaging factor. However, in most Florida pipe installations, due to flat landform, the pipe slopes are negligible. Therefore, abrasion is not a significant damaging factor in the state, and that mechanism was not considered here

For this set of experiments, SRAP quadruplicate specimens similar to section 5.1.2 were exposed to Solution S. The solution was constantly replenished at a slow rate of two liters per day. The results for the first 100 days of exposure indicated no significant difference between non-flowing and flowing conditions. As shown in Figure 24 and 25, the E_{OC} and measured currents of the flowing and non-flowing regimes were closely matched, indicating minimal

corrosion in all cases. Consequently, water replenishment does not appear to be an important variable in these phenomena, in agreement with the observation in the previous section.

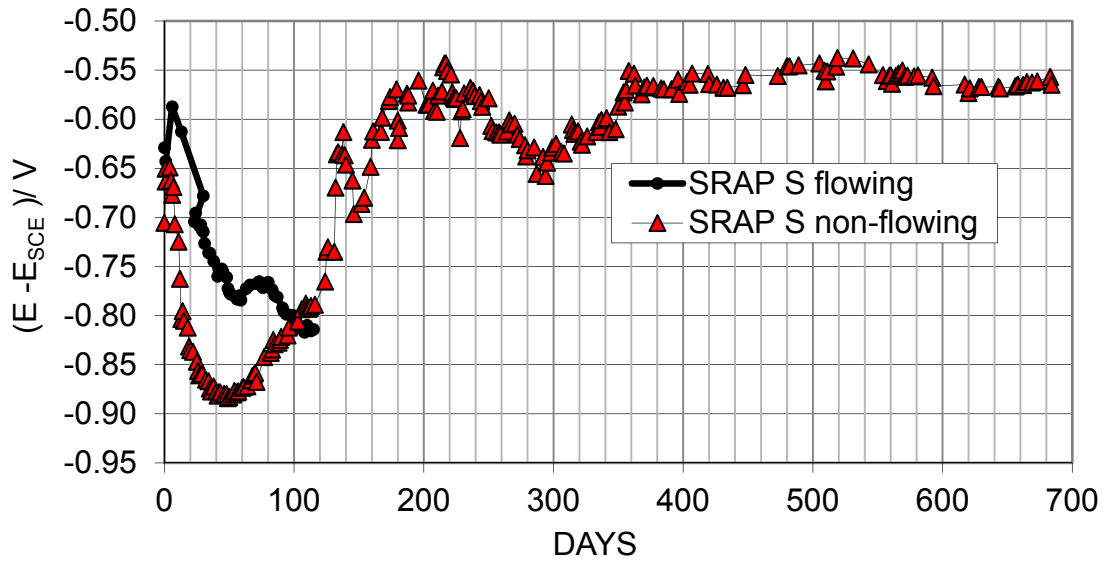

Figure 24: E_{OC} of SRAP in solution S -flowing vs. non-flowing condition.

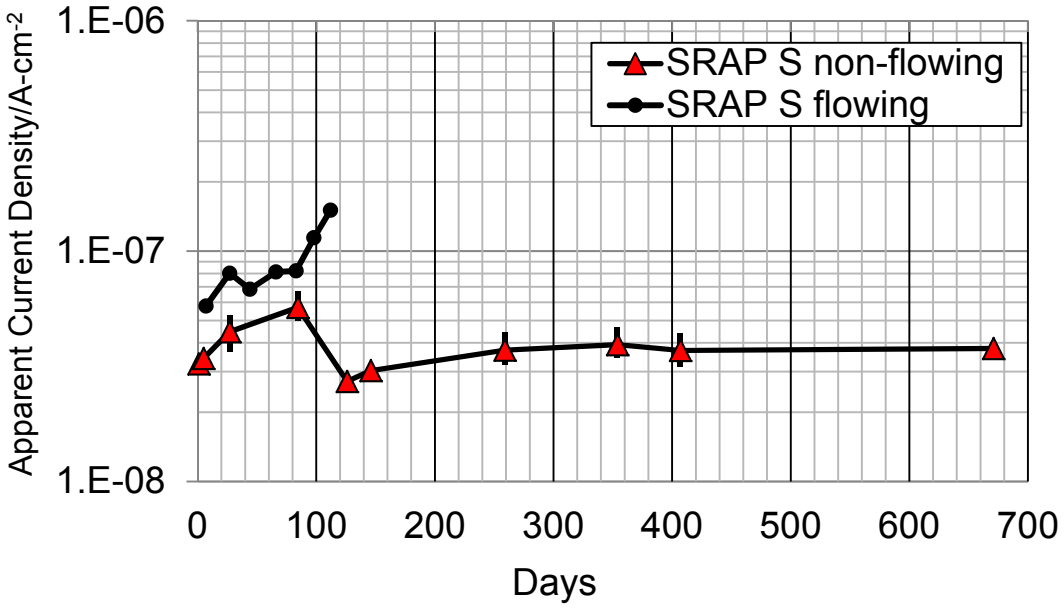

Figure 25: Apparent corrosion current density of SRAP in solution S -flowing vs. non-flowing condition.

5.2 Corrosion and Simulated Severe Manufacturing Distress

Aluminized steel with exposed cut edges replicates the severe manufacturing distress cases. Corroded exposed steel regions at cut areas are expected to be enhanced sites for the cathodic reaction, accelerating the corrosion of aluminum next to rusted areas. As aluminum loss continues, more steel substrate would be exposed developing a stronger cathode. This mechanism could result in lateral propagation of corrosion.

To test the above hypothesis, 8.5 x 9 in square specimens with cut edges were exposed to simulated water of S and S^+ in 5 gallon buckets. Each of these specimens was connected to a matching specimen with covered edges to measure galvanic action (macrocell currents) and to compare the corrosion behavior (Figure 26). The initial cathode to anode area ratio was extremely small, < 2 %.

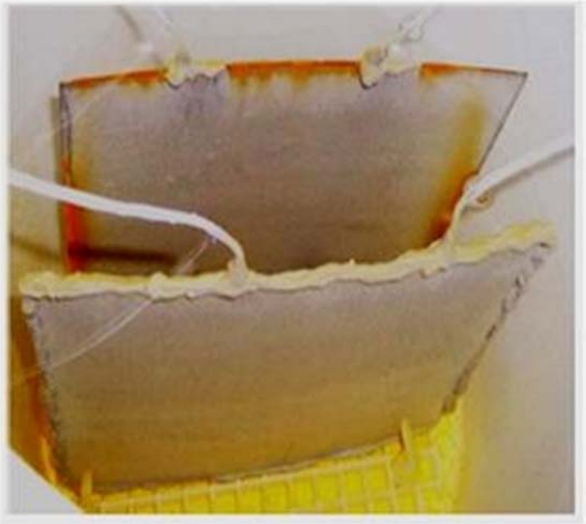

Figure 26 : Experiment set up for exposed cut edge experiment simulating severe manufacturing damage.

Figure 27 illustrate the E_{OC} evolution of the mixed pot of the system while Figure 28 shows the value of apparent corrosion current density and macrocell current. From the beginning of exposure, the galvanic current flowed between the

connected specimens. As expected, galvanic current measurements confirmed that the corroding steel edge was the cathode. This current gradually increased for the first 200 days as the cathode area increased (more steel corroded). During this period, the lateral discoloration and corrosion propagation of aluminum, initiating from the edges, continued.

At 175 days of exposure, the specimens were extracted for a few hours for surface inspections and were placed back into the cells in fresh solutions (Figure 29). Following the solution replenishment, the galvanic current between the sealed-edge and exposed-edge sections significantly increased for ~30 days; this increase was accompanied with an open circuit potential drop in all cells (Figure 27). It appears that the process of extraction and solution replenishment may have removed some of the iron corrosion product on the edges of exposed-edge specimens; the rust previously may have hindered or slowed down the corrosion rate, and the removal of corrosion products provided fresh sites for corrosion progression. As the corrosion rate of exposed edges increased, aluminum tended to provide higher galvanic protection by sending greater current.

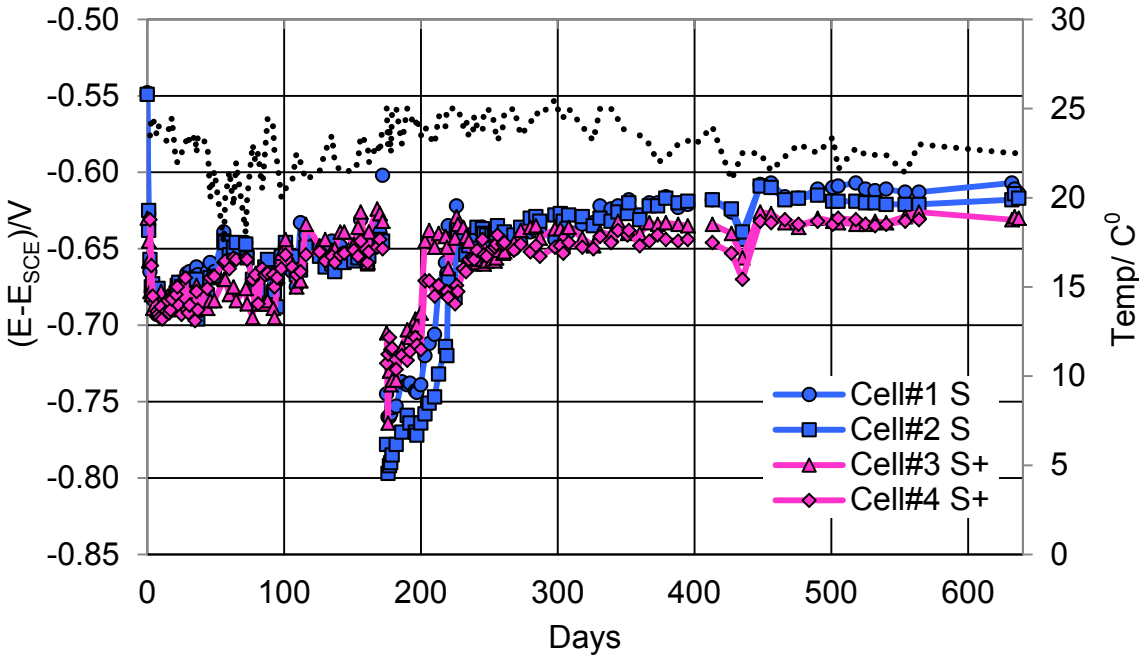

Figure 27: E_{OC} of open cut edge experiments (specimens taken out at 175 days).

After 200 days of exposure, where much of aluminum areas were discolored, the galvanic current gradually decreased with time to low values. The reduction of galvanic corrosion rate may indicate some surface alteration process that hinders the rate of the anodic reaction on the aluminum surface. In any event, the galvanic protection although present from the beginning of the exposure, was not sufficient to provide full protection of steel at open edges even for such small area fraction of cathode to anode. This occurrence is consistent with the presence of rust at the edges, and the less negative mixed potential values that approaching the typical potential of corroding steel in neutral water (McCafferty, 2010).

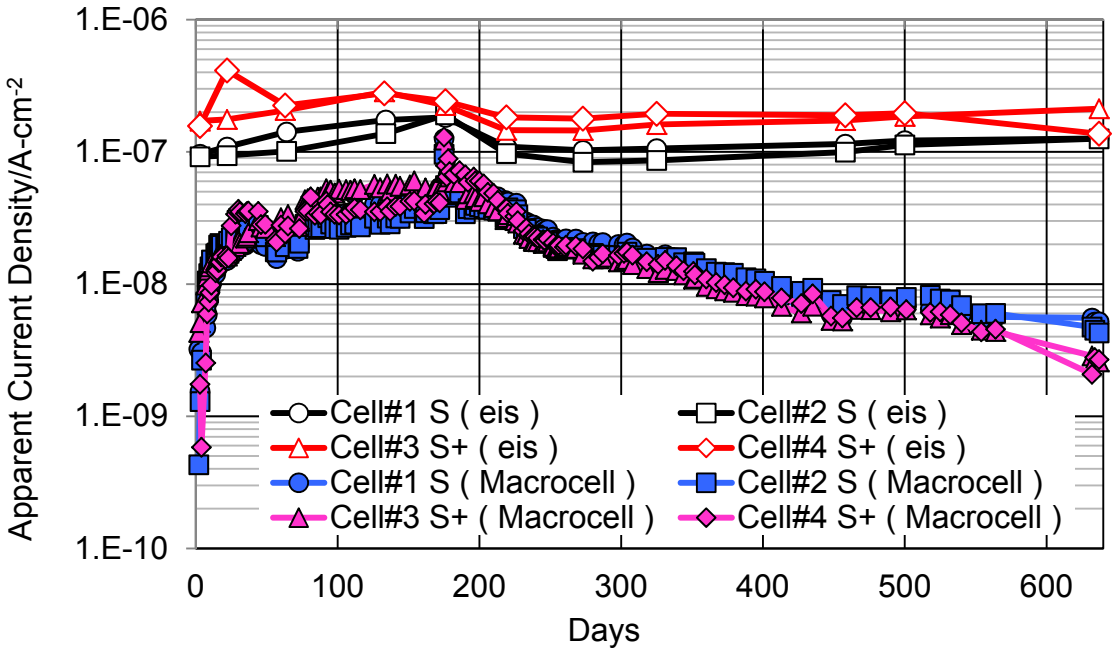

Figure 28: Micro cell current vs. apparent corrosion current density obtained from EIS tests.

The corrosion current density measured by EIS tests indicates a low but relatively constant corrosion rate. It should be indicated that for the calculation of this current density, the entire area of the anode (aluminum) was considered. However, if one only considered the narrow discolored areas of aluminum immediately adjacent to corroding steel the corrosion rate would be more than one order of magnitude greater. Determination of nominal corroding area to be used for corrosion current density is a difficult task as this area changes with time. Another complication in interpreting the EIS data is the effect of a corroding cathode (steel) that is not stationary as its area changes by time. These factors need consideration in subsequent investigations.

In summary, after about two years of exposure the evidence shows that the cut edges corroded readily in both solutions S and S+ , indicating inefficient aluminum galvanic protection even in the more aggressive environment.

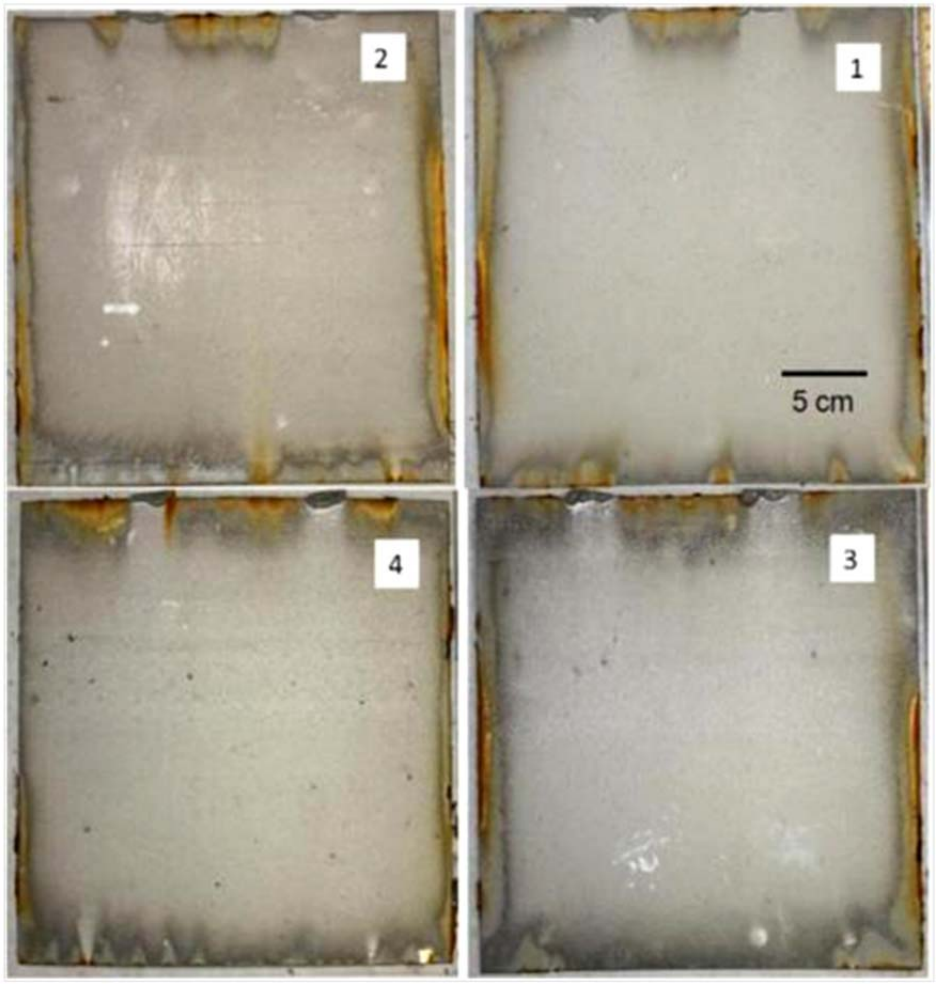

Figure 29 : Exposed cut edge experiment: Specimens extracted from solution S (top) and solution S+ (bottom). Lateral progression of corrosion is observed.

6. MECHANISM OF CORROSION PERFORMANCE IN WATER CONTACTING SAND AND LIMESTONE

In this other major area of the work experiments are conducted to elucidate the mechanism responsible for Mode B corrosion. Accordingly, the corrosion behavior of aluminized steel was evaluated in water in contact with clean sand as a relatively neutral medium serving as a control, and in water contacting limestone.

6.1 Corrosion in Sandy Soil

According to the U.S. Department of Agriculture (2003), Myakka fine sand has been recognized as the official native soil of Florida in 1989. Myakka fine sand covers more than 1.5 million acres of Florida's land and does not occur in any other states. Myakka, an Indian word for Big Waters, has a grey fine sand surface, light gray find sand subsurface layer, dark reddish brown fine sand with organic stains subsoil, and finally, yellowish brown fine sand substratum layer. To simulate the basic soil condition in Florida, two sets of experiments with silica sand and distilled water were designed. In the first series, as-received specimens (2 by 3") were cut from flat aluminized sheet stock; the edges of specimens were covered with epoxy. These specimens were exposed to fully soaked sand in cells configured as shown in Figure 30A. In these cells the distilled water was standing 2" above the sand to insure the full saturation. Measurements of water pH and conductivity were taken by immersing the corresponding probes sensing elements in the excess water above the sand. Results as function of exposure time are shown in Figures 31-32.

In the second series of experiments, similar specimens were placed in plastic cylinders that had tiny holes covered with filter paper at the bottom. The cells were filled with sand and were placed in a container filled with water up to half the height of cylinder Figure 30B. The specimens inside the cells were

located above the water line to provide a moist sand condition where the pores are not saturated. This condition was intended to increase the opportunity of corrosion by increasing oxygen access.

In both series, E_{OC} and EIS measurements were conducted to determine the corrosion regime and apparent rate of corrosion of the aluminized steel specimens. Results for triplicate specimens in saturated sand and quadruplicate specimens in moist sand conditions are presented in Figures 33 and 34.

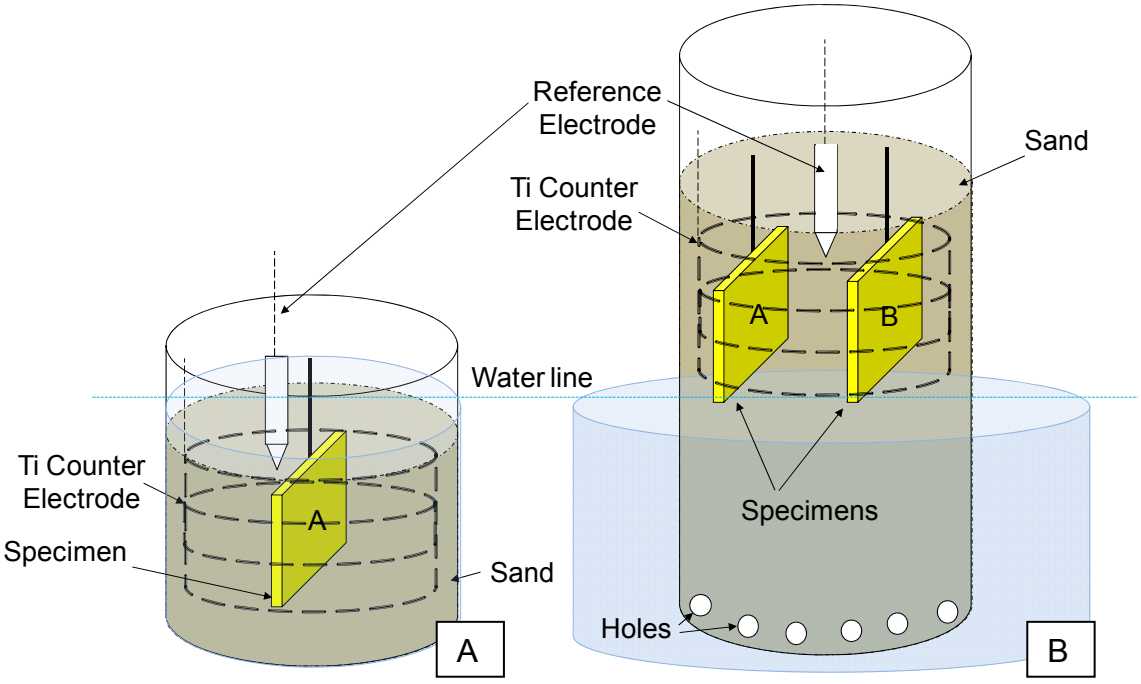

Figure 30: Sand experiment set up. A: Saturated sand experiment; B: moist sand experiment.

As indicated by pH and conductivity measurements, the near neutral environment in these tests, resulted in extremely low corrosion rates of < 1 µm/yr for both saturated and moist sand experiments Figure 34. While infrequent pits were observed on the surface of some specimens, in general the extracted specimens show no sign of severe corrosion. A typical metallographic cross-section of the specimen showing negligible wastage is given in Figure 35.

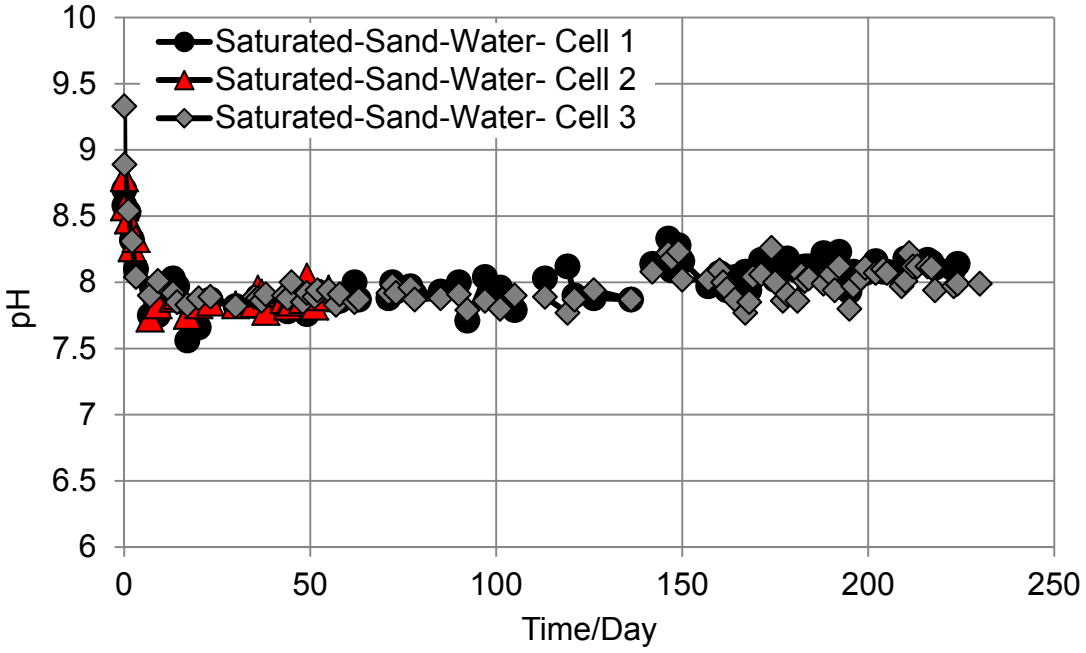

Figure 31: pH measured for triplicate specimens in saturated sand experiment.

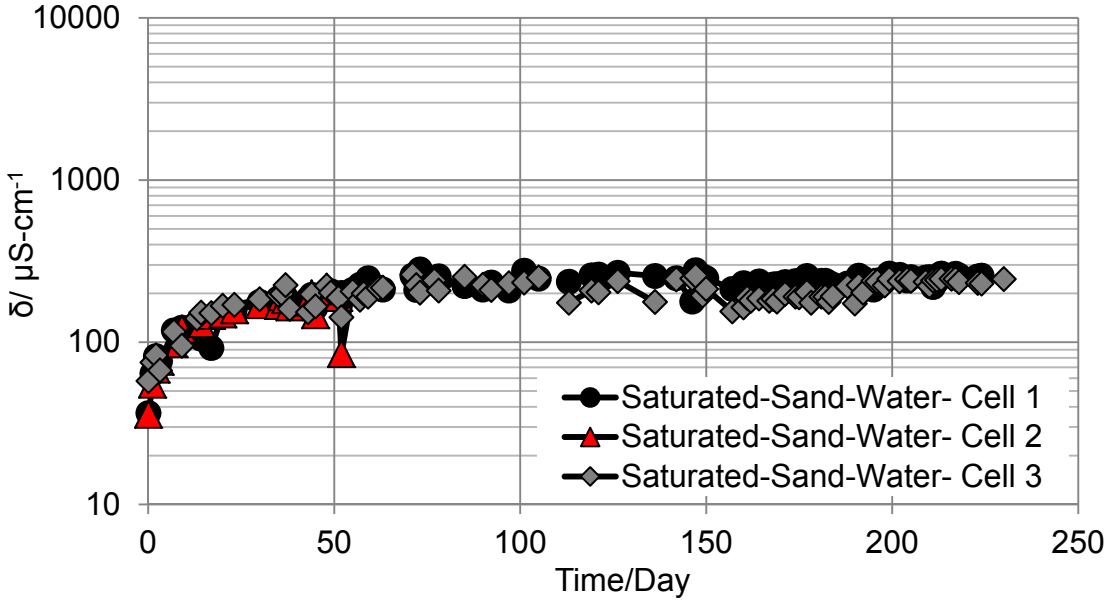

Figure 32: Conductivity measured for triplicate specimens in saturated sand experiment.

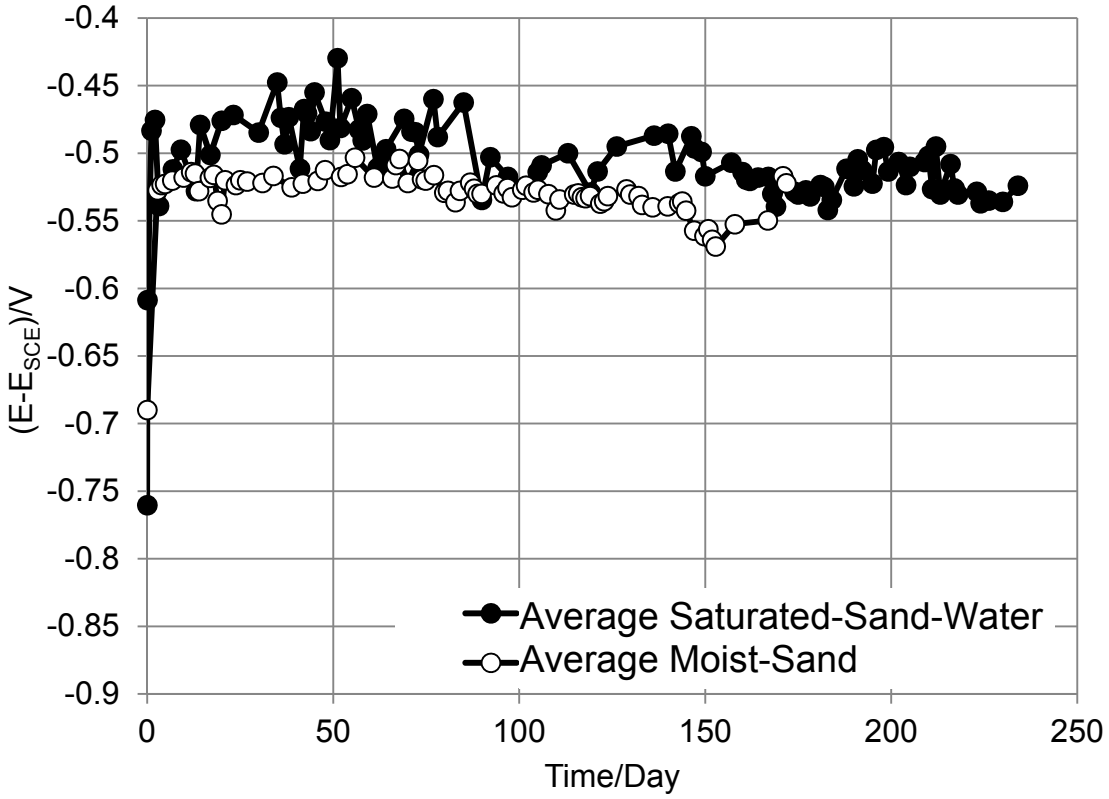

Figure 33: Average E_{OC} in saturated sand and moist sand experiment.

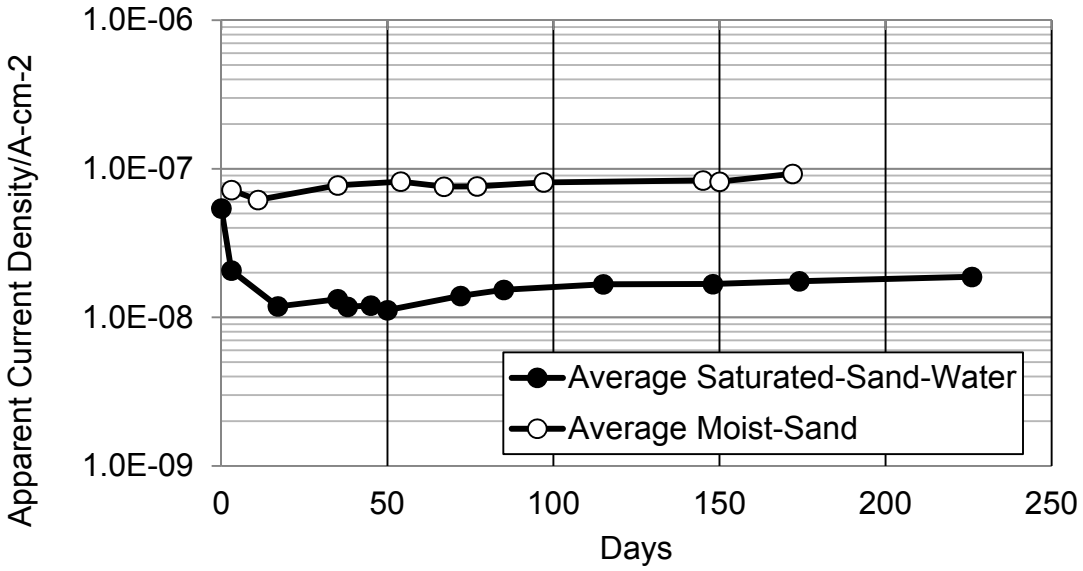

Figure 34: Average apparent current densities in saturated sand and moist sand experiment.

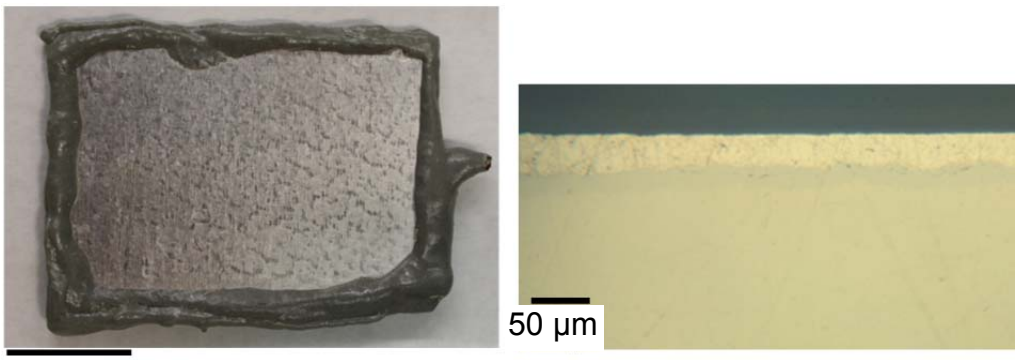

Figure 35: Bright appearance of specimen after exposure 250 days of exposure to water in sand medium (left); metallographic cross-section showing no significant aluminized layer consumption (right).

6.2 Corrosion in Limestone Backfill

6.2.1 Introduction

Construction aggregates complying with ASTM C568-96 for bedding and backfill of pipes are often used to provide good structural support (Figure 16). Among these aggregates, crushed limestone (mostly $CaCO_3$) is frequently used for its availability (1.17 billion metric tons production in US in 2009) and cost effectiveness (Virta, 2010). The pipe in the Jacksonville SR 212 Mode B corrosion incident (Table 1) was placed in limestone, and as noted in the introduction complete penetration of the coating and mild steel substrate, starting from the soil side, took place in only 3 years at localized spots over a > 10 m long section of pipe. As detailed in section 2, metallographic cross-section of a field sample indicated widespread consumption of the outer aluminum layer, a less affected intermetallic inner layer, and severe undercutting attack of the steel substrate. Chemical tests of water in the pipe (in contact with external water through the wall perforations) showed insignificant amount of aggressive ions such as chloride and sulfate at the site.

A hypothesis for the appearance of Mode B corrosion can be proposed whereby the dissolution of limestone backfill in the soil side water may have generated a high pH environment beyond the regime for stability of the aluminum passive film. A possible objection to that explanation is that water in contact with limestone in an open system equilibrated with atmospheric CO_2 develops only a mildly alkaline pH, typically ~8.3, (Snoeyink and Jenkins, 1980) that is virtually non-aggressive to a passive film on aluminum. However, previous studies on the utilization of limestone contactors for water treatment (Letterman, 1983; Letterman et al., 1991) showed dissolution of calcium carbonate in a closed system may increase the pH beyond 9. In the case of AST2 pipes in limestone backfill, slowly flowing water (e.g., rain) that is not given enough time for equilibration could approach closed system conditions and result in significant corrosion. These alternatives needed evaluation.

Therefore, the objective of this part of the work was to determine whether contact with limestone in flowing water could result in pH elevated enough for rapid corrosion of aluminized steel such as that observed in the field, and to further understand the mechanism of that corrosion. The findings merit consideration to assist in updating specifications for installation and use of backfill materials for aluminized steel culvert pipes.

6.2.2 Experimental Procedure

Laboratory experiments were conducted using 5 cm by 7.6 cm specimens (exposed area on two sides ~77 cm^2) cut from as-received AST2 gauge 16 (1.6 mm thick) flat sheet stock. A contact wire with insulation sheath was either spot welded or soldered to one of the edges. All the edges and wire connection were covered with two-component epoxy allowed to set for 24 hr. Then the exposed metallic surfaces were degreased with ethanol and stored in a desiccator prior to immersion.

The immersion cells (Figure 36) were upright cylinders made of acrylic glass, 10 cm internal diameter and 10 cm high. The lower 8 cm contained ~0.8 kg of limestone crushed to a sieve size between 1 cm and 3 cm, in which the specimen was embedded so its surface was in direct contact with multiple limestone particles. The composition of the rock used was tested in accordance with ASTM C1271 and confirmed to be ~97 wt% $CaCO_3$, comparable to commonly reported values for limestone (Boynton, 1980) The feed water was commercially supplied distilled water of resistivity > 50 kΩ-cm, representing rural rainwater (Sequeira and Lung, 1995). The feed water was held in a tank that allowed initial equilibration with atmospheric CO_2. Peristaltic pumps feed that water into each cell at a rate of ~2 liter per day. The water entered the cell at the lower end, ran in contact with the fully immersed specimen and the limestone, and was removed through an opening level at the top of the limestone fill. The chosen flow rate was intended for dissolution of limestone while avoiding excessive introduction of additional CO_2 from air into the cell solution, approximating a post-dissolution close system condition. A total of 14 specimens were tested in these flowing conditions. The pH, conductivity, and open circuit potential (E_{OC}) measurements were taken daily.

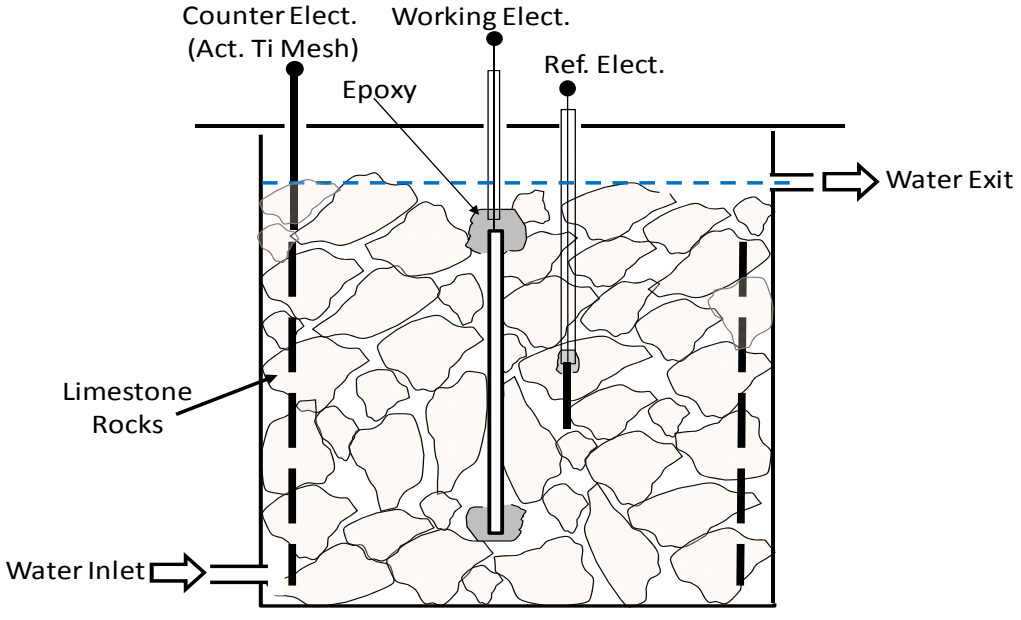

Figure 36 : Limestone-cell configuration.

For electrochemical measurements a titanium mesh with mixed metal oxide surface activation was placed all around near the inner wall of the cell to serve as a counter electrode. A similarly activated titanium rod 3 mm in diameter and 50 mm long was placed parallel to the specimen surface halfway to the counter electrode mesh, to serve as a low impedance temporary reference electrode (Castro et al., 1996). It was periodically calibrated against a SCE. All potentials reported here are in the SCE scale. Electrochemical impedance spectroscopy (EIS) measurements were periodically obtained for 8 of the specimens at the E_{OC} with a Gamry™ Ref. 600 potentiostat in the frequency range from 10 mHz to 100 kHz using sinusoidal signals of 10 mV rms amplitude. All tests were conducted at the room temperature. After exposure, the specimens were extracted and inspected for crevice corrosion. No crevice corrosion indications were observed in any cases. The tests and results for the first ~150 days are presented here.

Control specimens were exposed and tested in similar cells where the feed water was allowed to reach atmospheric equilibrium and not replenished.

6.2.3 Results and Discussion

In the cells with no flowing water the pH decayed to < 8.5 after one day and reached terminal values ≤ 8.3 afterwards. These values approximate the expected condition, noted earlier, for water in contact with limestone and equilibrated with atmospheric CO_2. Notably, the pH within the flowing water cells was found to have a stable value of ~9.3 starting with the first day of exposure. Computational chemical equilibrium model calculations using the program MINEQL$^+$ (Schecher and McAvory, 2003) indicated that the pH for water at 25 ^oC in contact with solid calcium carbonate, but without contact with atmospheric CO_2 (closed system) would be 9.91. If the water was assumed to be in equilibrium with atmospheric CO_2 before, but not after contact with calcium carbonate the computed result was only slightly smaller, pH = 9.84 indicating that any

atmospheric CO_2 present in the feed water before entering the cells should not be highly consequential. The pH ~ 9.3 value in the flowing water cells is therefore indicative that the conditions tend to approximate those of a closed system, where the interaction with atmospheric CO_2 cannot keep pace with the dissolution of limestone in the inflowing water.

Consistent with the resulting mild conditions, corrosion in the cells with no flowing water was relatively unimportant during the test period and those results will not be further addressed. In contrast, and as expected from the high solution pH, rapid corrosion of the aluminized coating took place in the flowing water cells. Direct observation of extracted specimens revealed that severe coating damage and surface discoloration took place starting after a short (about two weeks) exposure. Metallographic and SEM observations confirmed severe loss of aluminized coating later on, as illustrated in Figure 37. As shown there, the coating loss was rather generalized as opposed to sharply concentrated in the form of pits. The corrosion products (dark gray) stayed in place; Al-Fe intermetallic particles remained uncorroded in the matrix similar to observations in the field sample.

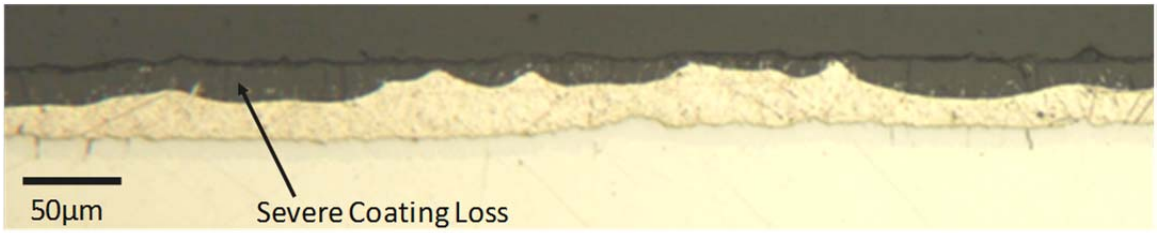

Figure 37 : Coating condition after ~150 days exposure to flowing water.

The E_{OC} initially decreased and reached a minimum (~ -1 V_{SCE}) indicative of highly active aluminum corrosion after about the first two weeks of exposure (Figure 38).

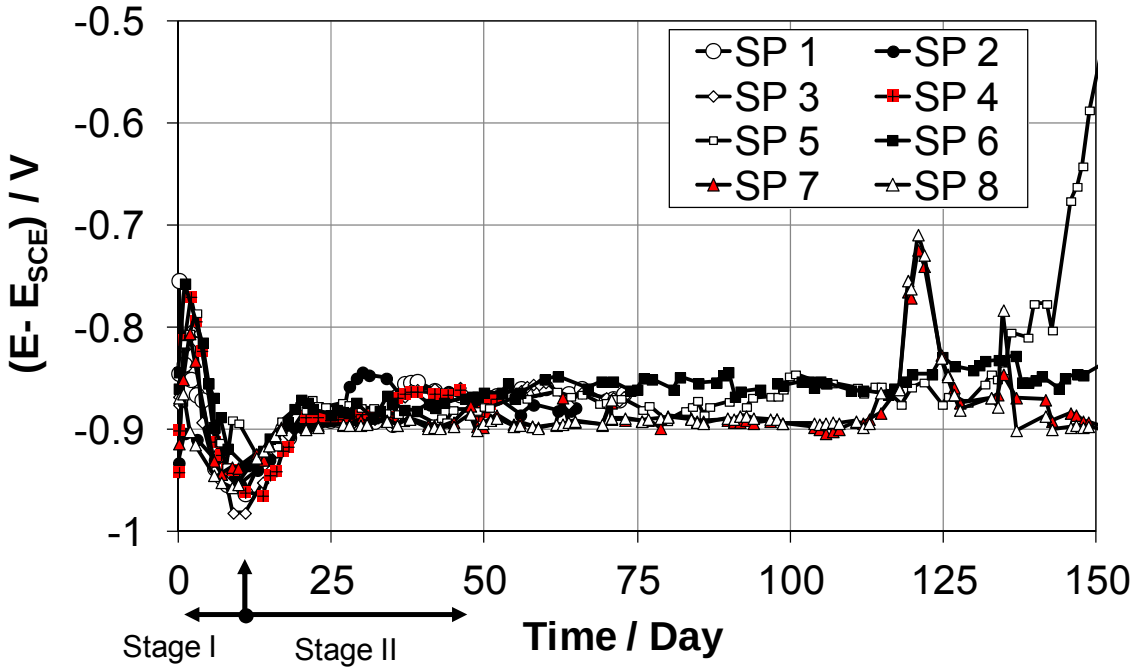

Figure 38: E_{OC} evolution; data from multiple replicate specimens.

Typical EIS behavior is shown for different exposure times in Figure 39. The high frequency loop (100 Hz - 100 kHz), only shown for day 1, reflects water dielectric properties apparent because of the high resistivity of the solution and was omitted in subsequent analysis. The solution resistance corresponded to the real value of the impedance at ~100 Hz. Variations with time of the solution resistance stemmed from minor changes in feed water composition and were not of consequence to the following analysis. A nominal polarization resistance Rpn, serving as a rough inverse indicator of corrosion rate, was obtained by subtracting the solution resistance from the real part of impedance at 10 mHz. A strong decrease in Rpn was observed at about two weeks of exposure, indicating high corrosion rate (Figure 40) followed by a gradual recovery.

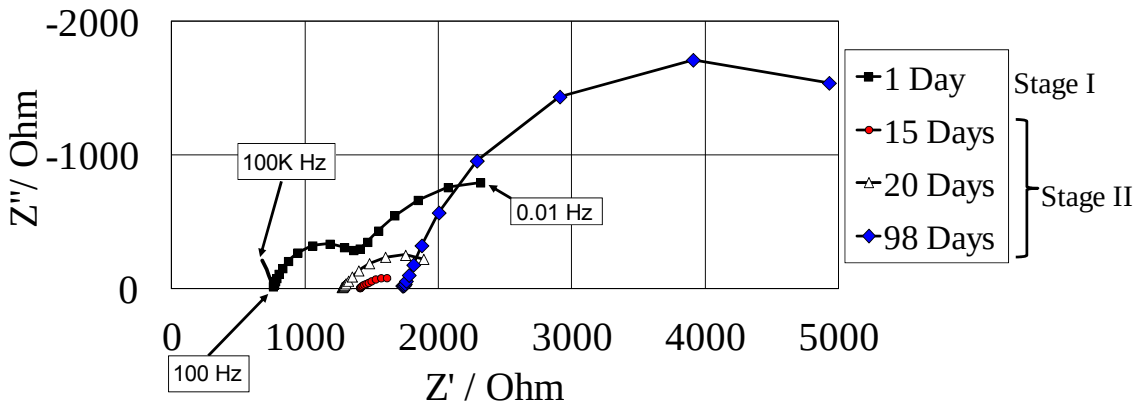

Figure 39: Typical EIS behavior of specimens exposed in limestone cells with flowing water. [10 mHz (last datum) to 100 kHz; 3 data/decade]. Specimen area was 77 cm^2.

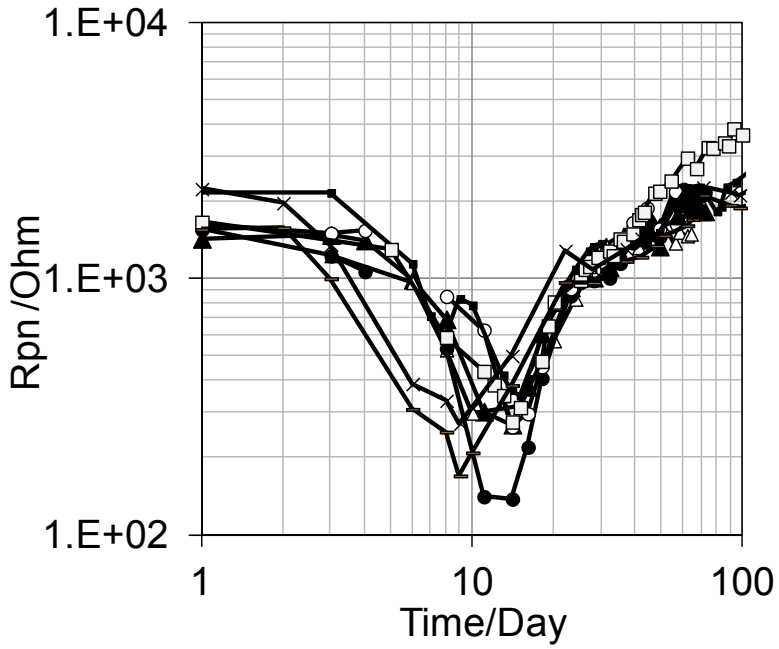

Figure 40: Nominal polarization resistance Rpn as function of exposure time. Area = 77 cm^2. Data from multiple replicate specimens.

To interpret the above results, the exposure time was divided into a Stage I, up to the time that nominal polarization resistance (Figure 40) reached its minimum value (~ first two weeks), and a subsequent Stage II where the nominal polarization resistance gradually increased. During Stage I the impedance

diagrams showed two clearly differentiated time constants. The faster time constant component was fit to a parallel Constant Phase Element (CPE) – resistor analog circuit as shown in Figure 41. The admittance of the CPE is $Y_0(j\omega)^n$ where Y_0 is the pre-exponential admittance term, ω is the angular frequency, and $0 \leq n \leq 1$.

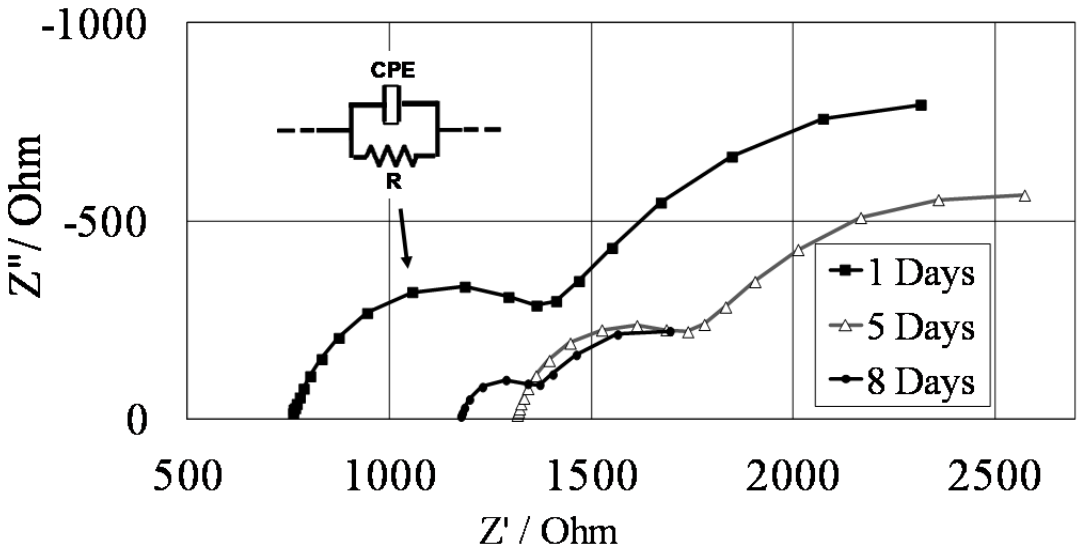

Figure 41: Stage I impedance behavior. [10 mHz (last datum) to 100 Hz; 3 data/decade]. Area = 77 cm^2.

For all specimens during Stage I the n value was typically >0.9, thus approaching ideally capacitive behavior with capacitance $C \sim Y_0 \sec^{(1-n)}$. C values were in order of 4 $\mu F\ cm^{-2}$ initially and increased with time. Such values are consistent with those expected for the capacitance of naturally formed aluminum passive films (Scully, 1993; Bessone et al., 1992). An estimate of the nominal thickness (d) of the film during Stage I was made using:

$$d = \varepsilon_0 \bullet \varepsilon \bullet A / C$$

where

ε is the dielectric constant of the passive film (estimated to be ~8) (Scully, 1993),

εo is the permittivity of free space ($8.85 \bullet 10^{-14}$ F/cm), 99

A is the area of the metal coating (~ $77 cm^2$).

The nominal film thickness is plotted as function of time in Figure 42 for multiple replicate specimens. The initial thicknesses were about 2-3 nm thick, comparable with values reported in previous studies (Scully, 1993; Bessone and Salinas, 1992). The values decreased with time and reached atomic dimensions (e.g., ~0.2 nm) after about 2 weeks. That condition may be viewed as being indicative of full consumption of the film at that time. Such interpretation is consistent with the concurrent strong drop in nominal polarization values (onset of severe corrosion), lowered E_{OC} (approaching the potential of actively corroding aluminum), and the appearance of a light grey shade on the surface of the specimens at the end of Stage I.

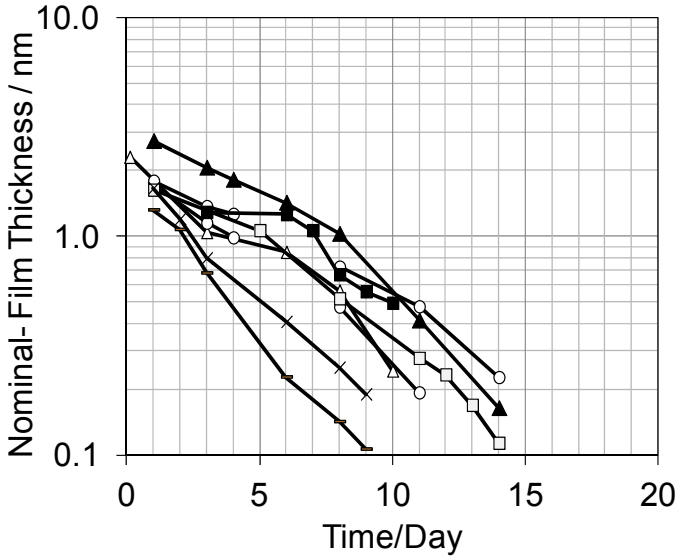

Figure 42 : Nominal film thickness during Stage I. Data from multiple replicate specimens.

As aluminum corrodes further (Stage II), the corrosion products are retained in the form a growing layer that, while not highly protective, may act as an increasingly thick barrier to the diffusion of reacting species. The subsequent gradual decrease in corrosion activity during Stage II (inferred from the Rpn trend) may be interpreted as being the result of the growth of that corrosion product layer. If on first approximation the rate of corrosion is inversely

proportional to the thickness of the growing layer, then the rate would decay proportionally to the square root of time (Stoudt et al., 1995). To test that hypothesis, Rpn^{-1} was plotted in log-log scale as function of $(t-t_0)^{½}$ where t is the exposure time and t_0 the time for the beginning of Stage II. The resulting combined graph for the data from all available specimens up to 150 days of exposure is presented in Figure 43. The overall slope was -1.19, approaching the ideal value of -1 that would correspond to the proposed scenario. The validity of this semiquantitative treatment is the subject of continuing work for refined interpretation of the EIS behavior, including proper correlation between polarization or charge-transfer resistance with corrosion rate, and identification of the ruling corrosion reactions in Stage II.

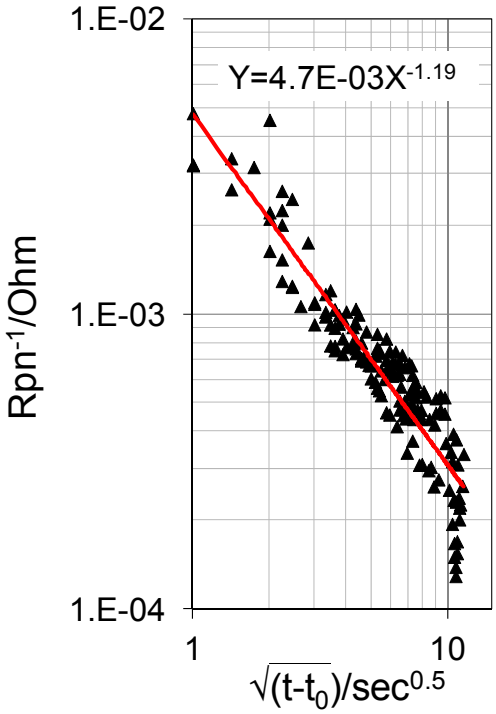

Figure 43: Corrosion rate vs. square root of time after the full dissolution of oxide protective film. Combined graph with data from multiple replicate specimens.

The findings to date, while preliminary, suggest the overall corrosion progression in flowing water summarized in Figure 44.

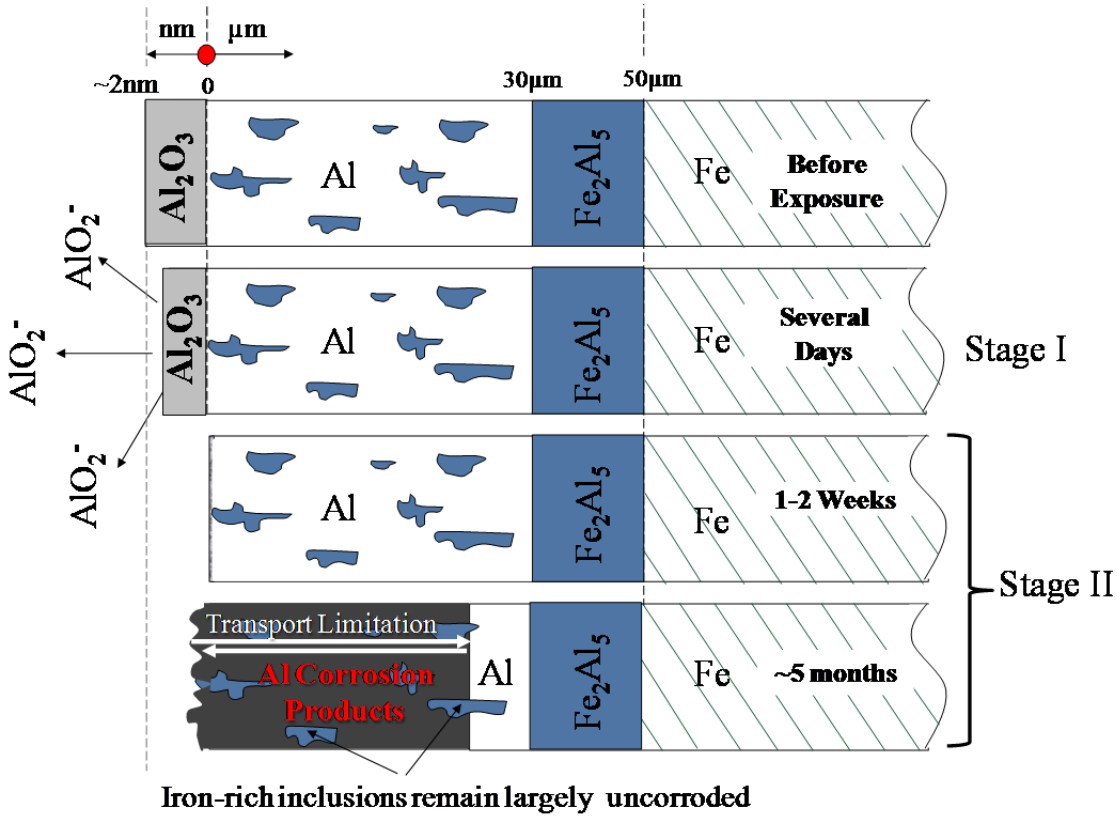

Figure 44: Scenario of corrosion progression under flowing water condition.

During Stage I the passive film on the outer layer of the aluminized coating is consumed by interaction with the high pH generated by dissolution of limestone under near-closed system conditions. After 1-2 weeks the film is completely consumed and active corrosion of the aluminum begins (Stage II) at a high rate. Corrosion products remain in place and transport limitation of one or more of the species responsible for the rate of corrosion ensues in an increasingly thick film. Nevertheless, after several months of exposure a significant fraction of the aluminized coating had been consumed. Aluminate inclusions and the inner aluminized layer are less attacked. Corrosion of the underlying carbon steel, not addressed in the present experiments, is expected to take place at a later date, but the observed attack of the aluminized coating in such short time portends a dramatic reduction in the life expectancy of the pipe

compared to the desired performance. The results thus provide an explanation for the early damage observed in the field.

More detailed analysis of the experimental results presented here has taken place in follow up work after the completion of this project, with findings largely in agreement with the above interpretation. A description of that continuation work is given by Akhoondan (2012).

7. GENERAL DISCUSSION

7.1 Mode A Corrosion Issues

This investigation has provided further evidence (sections 2 and 5) that the rib deformations of SRAP are prone to corrosion even in the absence of evident manufacturing defects. Experiments with heavily deformed aluminized steel performed in the previous investigation (section 3) and expanded here showed that severe corrosion can develop in heavily mechanically formed regions. The preliminary experiments with small specimens (section 5.1.1) showed also indications of preferential corrosion at normally formed ribs in pipe manufactured recently to carefully implemented standards. However, the more extensive experiments with large surface area samples of similarly newly produced pipe in both stagnant and renewed water (sections 5.1.2 and 5.1.3) did not show severe corrosion at the ribs. In those more comprehensive tests, SRAP showed some rib corrosion but overall did not perform markedly different from regular corrugated pipe, which is not subject to the severe local forming needed for SRAP.

The bending radius measurements reported in section 3 provided no indication of distinctly sharper radii in the ribs of pipe that experienced heavy Mode A corrosion than in more recent pipe produced under expected careful quality control. Thus, those measurements failed to provide support to the hypothesis that much of that corrosion was due to routinely sharper radius settings when forming the earlier pipe. Since the most severe Mode A corrosion incidents were associated with gross manufacturing defects (i.e., helical cuts), the above findings suggest that preferential rib corrosion in those cases reflected more some sort of associated production deficiency than a feature inherent to the rib making process. Such deficiency (for example tearing from stuck rollers or inadequate lubrication) could have involved in some of the ribs mechanical

coating distress significantly beyond that which is found in normal forming, resulting in conspicuous corrosion damage.

The experimental findings did not provide enough evidence to support the hypothesis that Mode A corrosion could have been mitigated by a somewhat more aggressive environment, which would have partially activated the aluminized layer surface and hence galvanically protected the exposed steel. As shown in section 5.1.2, tests of large SRAP specimens with the most aggressive S+ solution showed only marginally more negative potentials than parallel tests with the S solution, and visual appearance as well as electrochemical impedance results were not dramatically different in comparison specimens exposed to both solutions. The small size preliminary experiments showed no significant S /S+ solution differentiation either. In all those tests exposed steel was limited to small imperfections present in the as received material.

The exposed edge experiments (section 5.2) were specifically designed to reveal to what extent galvanic protection could be provided by the aluminized layer to a large area of exposed steel, as it would be present in the case of a helical cut resulting from manufacturing deficiency. The experiments confirmed that some protecting galvanic current was delivered to the steel, but also indicated that the amount of protection was insufficient to substantially arrest corrosion of the steel. Importantly, these tests too revealed no strong differentiation between the S and S+ solution exposures thus not supporting the hypothesis that moderately more aggressive waters would have a strong beneficial effect in mitigating exposed steel corrosion. It is noted that while the protective galvanic effect (regardless of how aggressive the solution is) was not substantial in the cut edge case, it may have had a more important mitigating effect for the smaller flaws present in the surface of as-received material. Such mitigation may have contributed to the lesser amount of rib corrosion encountered in the large specimen experiments (sections 5.1.2 and 5.1.3) than in the preliminary tests with small specimens (section 5.1.1). The latter had about

half the ratio of ribbed surface to smooth surface than the former, with consequent lesser expected galvanic protection of any steel exposed at the rib deformations.

In summary, the findings from this work continue to suggest that much of the corrosion damage observed in the Mode A incidents was promoted more by manufacturing deficiencies, and less by any possible inherent susceptibility of corrosion at the ribs of SRAP that is produced following appropriate quality control. The work confirmed the presence of some galvanic protection to exposed steel, but no particular protection enhancement was found by exposure to a lower resistivity environment.

7.2 Mode B Corrosion Issues

The results of the experiments in section 6.2 showed that high pH values, sufficient to cause dissolution of the passive film on aluminum, can develop under exposure of limestone to flowing natural water. In these conditions, extensive loss of coating was observed over a short time period. In contrast, exposure to water in contact with sand (section 6.1) did not result in alkaline conditions and aluminized steel (in the absence of mechanical deformation) remained essentially corrosion free.

Corrosion of the aluminized film in the limestone medium with renewed water took place in two consecutive stages. In Stage I the passive firm was consumed by interaction with the high pH medium. In Stage II active corrosion of the outer layer aluminized coating took place with formation of an increasingly thick corrosion product layer with associated transport limitation.

The findings substantiate for the first time an important vulnerability of aluminized steel in limestone soils and provide an explanation for the onset rapid

deterioration observed at the field. It is noted that the experiments did not extend to a period where the underlying steel is corroded, but that event is to be expected once the protective aluminized layer is compromised. With the environment remaining alkaline, it is natural to anticipate penetration of the steel to be mostly localized since that mode of corrosion is prevalent for steel under those conditions.

The findings provide strong evidence in support of service guidelines to disallow the use of limestone bedding for aluminized steel pipe, including SRAP. Consideration should be given to examine the need of extending that provision to the use of solid aluminum alloy pipe. Other backfill materials such as crushed concrete could create a high pH environment by a similar mechanism as that considered here. The potential for such occurrence should be investigated and service guidelines for those materials revised accordingly if warranted.

8. CONCLUSIONS

1. Spiral Ribbed Aluminized Pipe (SRAP) premature corrosion incidents have occurred in two modalities. Mode A is associated with extensive corrosion at or near the ribs and has taken place in near-neutral regular soil environments. Mode A has been often associated with gross manufacturing defects (i.e., helical cuts). Mode B took place in pipe in contact with limestone backfill and corrosion damage was in the form of perforations not preferentially at the ribs and not necessarily associated with other deficiencies. Both modes resulted in severe corrosion after only a few years of service.

2. Corrosion comparable to that in Mode A was replicated in aluminized steel that has been severely deformed to expose significant amounts of steel at aluminized layer breaks. However, moderately strong deformation such as that involved in the normal forming of SRAP ribs did not consistently result in severe corrosion. In comparison tests SRAP showed some rib corrosion but overall did not perform markedly different from regular corrugated pipe, which is not subject to the extent of forming needed for SRAP.

3. Experiments confirmed the presence of some galvanic protection to exposed steel in conditions comparable to those of Mode A, but no particular protection enhancement was found by exposure to a lower resistivity environment.

4. Overall the findings continue to suggest that much of the corrosion damage observed in the Mode A incidents was promoted more by manufacturing deficiencies, and less by any possible inherent susceptibility of corrosion at the ribs of SRAP that is produced following appropriate quality control.

5. Experiments to explore the causes of Mode B corrosion showed that high pH values, sufficient to cause dissolution of the passive film on aluminum, can develop under exposure of limestone to flowing natural water. In these conditions, extensive loss of coating was observed over a short time period. In contrast, exposure to water in contact with sand did not result in alkaline conditions, and aluminized steel, in the absence of mechanical deformation, remained essentially corrosion free.

6. Corrosion of the aluminized film in the limestone medium with renewed water, approximating Mode B conditions, took place in two consecutive stages. In Stage I, the passive film was consumed by interaction with the high pH medium. In Stage II, active corrosion of the outer layer aluminized coating took place with formation of an increasingly thick corrosion product layer with associated transport limitation.

7. The findings substantiate for the first time an important vulnerability of aluminized steel in limestone soils and provide an explanation for the onset of rapid deterioration observed at the field under Mode B.

8. The findings provide strong evidence in support of service guidelines to disallow the use of limestone bedding for aluminized steel pipe, including SRAP. Similar provisions for crushed concrete merit consideration.

REFERENCES

AASHTO (2008), *AASHTO M 274: Standard Specification for Steel Sheet, Aluminum-Coated (Type 2), for Corrugated Steel Pipe*, American Association of State Highway and Transportation Officials, Washington, DC.

AK Steel Corporation (2012). *Aluminized Steel Type 2: Product Features* (Revision 06.17.12), West Chester, OH. http://www.aksteel.com/pdf/markets_products/carbon/AK%20AlmT2%20Features%20061712.pdf (accessed November, 2012)

Akhoondan M. (2012), *Corrosion Evaluation and Durability Estimation of Aluminized Steel Drainage Pipes*, Ph.D. Dissertation, University of South Florida, Tampa, FL..

Akhoondan M., Sagüés A. (2007), *Corrosion of Mechanically Formed Aluminized Steel*, Student Poster/2007, Presented during the 2007 NACE International Annual Meeting, Nashville, TN, 2007.

Akhoondan M, Sagüés A., Cáseres L. (2008), Corrosion Assessment of Mechanically Formed Aluminized Steel, Paper No. 08396, *Corrosion/2008*, NACE International, Houston, TX, 2008.

American Society for Metals (1972), *Metals Handbook*, 8th Ed., Vol. 7, ASM International, Metals Park, OH.

An J., Liu Y.B., Sun D.R. (2001), Mechanism of Bonding of Al–Pb Alloy Strip and Hot-Dip Aluminized Steel Sheet by Hot Rolling, *Materials Science Technology* 17, pp. 451-454.

Armstrong R.D., Braham V.J. (1996), The Mechanism of Aluminum Corrosion in Alkaline Solutions, *Corrosion Science* 38, pp. 1463-1471.

ASTM (2007), *A929/A929M-01, Standard Specification for Steel Sheet, Metallic-Coated by the Hot-Dip Process for Corrugated Steel Pipe*, ASTM International, West Conshohocken, PA.

ASTM (2010), *A760/A760M-10, Standard Specification for Corrugated Steel Pipe, Metallic-Coated for Sewers and Drains*, ASTM International, West Conshohocken, PA.

Bessone J.B., Salinas D.R., Mayer C.E., Ebert M., Lorenz W.J. (1992), An EIS Study of Aluminium Barrier-Type Oxide Films Formed in Different Media, *Electrochimica Acta* 37, pp. 2283-2290.

Bednar L. (1989), Galvanized Steel Drainage Pipe Durability Estimation with a Modified California Chart, Paper No. 88-0341, *68th Annual Meeting*, Transportation Research Board, Washington, D.C.

Boynton R. B. (1980), *Chemistry and Technology of Lime and Limestone*, John Wiley & Sons, New York, NY.

Cáseres L. (2007), *Electrochemical Behavior of Aluminized Steel Type 2 in Scale-Forming Waters,* Ph.D. Dissertation, University of South Florida, Tampa, FL.

Cáseres L. and Sagüés A. (2007), Galvanic Behavior of Type 2 Aluminized Steel in Simulated Natural Waters", *ECS Transactions* Vol. 13, Issue 13, pp. 147-157.

Cáseres L., Sagüés A.A. (2005), Corrosion of Aluminized Steel in Scale Forming Waters, Paper No. 05348, *Corrosion/2005*, NACE International, Houston, TX.

Castro P., Sagüés A ., Moreno E.I., Maldonado L., Genescá J. (1996), Characterization of Activated Titanium Solid Reference Electrodes for Corrosion Testing of Steel in Concrete, *Corrosion* 52, p. 609.

Cerlanek W.D., Powers R.G. (1993) *Drainage Culvert Service Life Performance and Estimation*, Report No. 93-4A, Florida Department of Transportation, Tallahassee, FL.

CONCORR Florida (2007), *Curlew Road Aluminized Steel Type II Pipe Failure Investigation*, Prepared for FDOT State Materials Office, Gainesville, FL.

Creus J., Mazille H., Idrissi H. (2000), Porosity Evaluation of Protective Coatings Electrodeposited on Steel, *Surface and Coatings Technology 130*, pp. 224-232.

Davis J. R., (2000), *Corrosion of Aluminum and Aluminum Alloys*, ASM International, Metals Park, OH, p. 26.

Federal Highway Administration (FHWA) (2000), *Durability Analysis of Aluminized Type 2 Corrugated Metal Pipe*, US Department of Transportation Report No. FHWA-RD-97-140, McLean, VA.

Florida Department of Transportation (FDOT) (2008), *Optional Pipe Materials Handbook,* Tallahassee, FL.

Gupta A., Kumar R. (2006), Formability of Galvanized Interstitial-Free Steel Sheets, *Journal of Materials Processing Technology*, 172, pp. 225-237.

Hong, Lim, Chung, Choi (2002), Texture and Corrosion Mechanisms of Aluminized Steel Sheets, *Material Science Forum*, 408-412, pp. 1031-1036.

Hwang, Song, Kim (2004), Effects of Carbon Content of Carbon Steel on Its Dissolution Into a Molten Aluminum Alloy, *Materials Science and Engineering* 390, pp. 437-443.

Johnsson T., Nordhag L. (1984), Corrosion Resistance of Coatings of Aluminum, Zinc and their Alloys: Results of Four Years' Exposure, *Interfinish 84*, 11thWorld Congress on Metal Finishing, Jerusalem, Israel, 21-26 October 1984, pp. 412-418.

Jones. D.A. (1996), *Principles and Prevention of Corrosion*, Prentice Hall, Upper Saddle River, NJ, pp. 75-113.

Kimoto H. (1999), Galvanic Corrosion Behavior of Aluminized Steel in Seawater, *Corrosion Engineering*, 48, pp. 579-588.

Kobayashi Sh., Yakou T. (2002), Control of Intermetallic Compound Layers at Interface Between Steel and Aluminum by Diffusion-treatment, *Materials Science and Engineering*, A338, pp. 44-53.

Legault R.A., Pearson V.P. (1978), Kinetics of the Atmospheric Corrosion of Aluminized Steel, *Corrosion* 34, pp. 344-348.

Letterman R.D. (1983) *Limestone Contactors for Corrosion Control in Small Water Supply Systems*, Final Report submitted to the U.S. Environmental Protection Agency, Drinking Water Research, MERL, Cincinnati, OH.

Letterman R.D., Driscoll C. T., Hadad M. (1991), Contactors-Steady-State Design Relationships, *Journal of Environmental Engineering*, ASCE, 117, pp. 339-358.

Li W., Liu S., Huang Q., Gu M. (2003), Hot-Dipped Aluminising (HDA) of a Low Carbon Steel Wire, *Materials Science and Technology* 19, pp. 1025-102.

Lucas K.A. and Clarke H. (1993), *Corrosion of Aluminum-Based Metal Matrix Composites*, p. 25, Research Studies Press LTD., New York, NY.

McCafferty E. (2010), *Introduction to Corrosion*, Springer; Washington, DC.

Mohanty (2000), Developments in Automobile Steel grades - Experience at TATA Steel, *Iron Steel Rev*. Pp. 19-27.

Molinas A., Mommandi A. (2009), *Development of New Corrosion/Abrasion Guidelines for Selection of Culvert Pipe Materials*, Final Report on Project No. CDOT-2009-11 to Colorado Department of Transportation, November 2009.

Morris G.E., Bednar L. (1998), *Comprehensive Evaluation of Aluminized Steel Type 2 Pipe Field Performance*, AK Steel Corporation, Middletown, OH.

Najafi T., Salem S., Bhattachar D., Salman B. (2008), *An Asset Management Durability of In-situ Pipe Repair*, Final Report on Project No. 0092-07-19 to Wisconsin Department of Transportation, June, 2008.

Najafi T., Harris W., Muszynski L., Alwood D., Mamaghani T., McBride D.,(2011), *An Asset Management Approach for Drainage Infrastructure and Culverts*, Final Report on BD75 977-38 to Florida Department of Transportation, November, 2011.

Pourbaix M. (1995), *Lectures on Electrochemical Corrosion*, p. 146, NACE International, TX.

Sagüés A. (2006), Electrochemical Impedance Spectroscopy Course Notes, University of South Florida.

Sagüés A.A., N. D. Poor, L. Cáseres, M. Akhoondan (2009), *Development of a Rational Method for Predicting Corrosion of Metals in Soils and Waters*, Final Report on Project No. BD497 to Florida Department of Transportation, Tallahassee, FL. http://www.dot.state.fl.us/research-center/ .

Sequeira R., Lung F. (1995), A Critical Data Analysis and Interpretation of The pH, Ion Loadings and Electrical Conductivity of Rainwater From The Territory of Hong Kong, *Atmospheric Environment* 29, pp. 2439-2447.

Schecher W. D., McAvory D. C. (2003), *MINEQL+: A Chemical Equilibrium Modeling System, Environmental Research Software*, Version 4.6 for Windows. www.mineql.com (accessed November 2012)

Scully J. R. (1993), Characterization of the Corrosion of Aluminum Thin Films Using Electrochemical Impedance Methods, *Electrochemical Impedance: Analysis and Interpretation, ASTM STP 1188*, J. R. Scully, D. C. Silverman, and M. W. Kendig, Eds., Philadelphia, PA, p. 276.

Snoeyink V. L., Jenkins D. (1980), *Water Chemistry*, John Wiley & Sons, New York, NY.

Stoudt M. R., Fink J. L., Dante J. F., Ricker R.E. (1995), Compatibility with Metals, Fire Suppression System Performance of Alternative Agents in

Aircraft Engine and Dry Bay Laboratory Simulations, *NIST SP 890*, Vol. 1, R. G. Gann, Ed., NM, Eds, p. 128.

Townsend H.E., Borzillo A.R. (1987), Twenty-Year Atmospheric Corrosion Tests of Hot-dip Coated Sheet Steel, *Materials Performance* 26, pp. 37-41.

United States Department of Agriculture (USDA) (2003), Natural Resources Conservation Service, *Soil Survey, Florida Counties*, 2003, Washington, DC.

Virta R. L. (2010), *2009 Minerals Yearbook*, U.S. Geological Survey, Washington, DC.